Indiana University-Purdue University Fort Wayne

Department of Electrical & Computer Engineering
&
Department of Mechanical Engineering

ENGR 410 - 411

Capstone Senior Design Project
Report #2

Project Title: IPFW Electric Vehicle

Project Website: http://ipfwev.com/

Faculty Advisors:

Dr. Hosni Abu-Mulaweh
Dr. Abdullah Eroglu
Dr. Hossein Oloomi

Team Members:

Andres Cobos
Mitchell Eilerman
Leandra Lee
Charles McIntosh
Austin Swihart
Josh Weaver

Date: December 8, 2015

Table of Contents

Acknowledgement

We would like to thank our advisors, Dr. Hosni Abu-Mulaweh, Dr. Abdullah Eroglu, and Dr. Hossein Oloomi, for all of their help and time with this project. We would also like to thank our consultant, Derek Krebs, for his expertise and assistance with the project. We would also like to thank the National Science Foundation for sponsoring this project with grant 1427809.

Abstract

The IPFW electric vehicle project is funded by the National Science Foundation (NSF). The goal of the design phase of the project was to obtain a feasible design for the creation of an electric vehicle. The design team had at its disposal a small off-road car designed by a team of IPFW students and faculty in 2008 for a Baja SAE competition. The car had a 10 hp Briggs & Stratton gas motor and a CVT. The team also had a four-quadrant bidirectional DC-DC converter designed by another team of IPFW students and faculty in 2014. The DC-DC converter was designed specifically as a drive system for an electric vehicle and includes a 5,000W brushless DC motor, two 12V lead-acid batteries, and an 87W solar panel. The team's goal was to design the integration of these two systems. The design needed to be developed within a fourteen-week timeframe, and the resulting design could not exceed $1,000.

The problem statement was designed to provide an overall description of the project's requirements as well as to determine which parameters are fixed and which may be changed in the design process. Relevant projects constraints, including those pertaining to safety, environmental, and economic concerns, were chosen so that potential solutions can be judged properly. The problem statement served as a blueprint for the entire design stage.

The next step was to generate solutions that satisfied the problem statement. In order to do this, multiple sessions of brainstorming were used to generate potential concepts. To facilitate this process, the vehicle was divided into four subsystems - the charging system, the DC-DC converter, the cooling system, and the control system. About two dozen concepts were generated by the group for each subsystem. These concepts were generally evaluated based on the problem statement criteria and the best three or four solutions for each subsystem were chosen to undergo more detailed analysis.

Once all subsystems had a few possible solutions, one concept was to be chosen for each. This process began by developing criteria with which to evaluate the concepts for each subsystem. These criteria were weighted based on their importance to the subsystem. Each team member rated each concept of the subsystems of their expertise. The final scores were then averaged and compared, resulting in a chosen concept for each of the four subsystems.

The final concepts were then researched in detail for the detailed design. Each concept was analyzed and important purchasing and design decisions made. Just as the problem statement served as a blueprint for the design of the electric vehicle, the detailed design now serves as a blueprint for the creation of the electric vehicle.

During the implementation of the design, the gas motor was removed from the mini-Baja vehicle and replaced with the electric motor. The batteries and DC-DC converter were positioned and mounted in the rear of the vehicle. A speed sensor and temperature sensors were installed throughout the vehicle. A stepper motor was implemented to enable speed control. Fins and fans were implemented for a cooling system for the

batteries. The existing Arduino microcontroller was used to interface all components of the vehicle. The solar panel was integrated into the charging system.

Testing of the vehicle was conducted to determine whether the vehicle met the requirements of the problem statement. The DC motor and batteries successfully met the requirement of working together to power the vehicle. The solar panel failed to meet the requirement of fully charging two batteries by exceeding the specified time by two hours. Likewise, the acceleration and top speed of the vehicle failed to meet the requirements of the problem statement. The requirement of an adjustable speed of the system was achieved with the compression of the driver operated pedal. The torque requirement of the problem statement could not be measured due to the absence of required tools. The cooling system of the vehicle successfully met the requirement of maintaining component temperatures below operating temperatures for optimal efficiency.

The $600 budget granted by the department for the project was exceeded with a total project cost of $2,040.25. The next phase of the electric vehicle project will be to implement cruise control as part of the speed control.

Section I: Problem Statement

The proposed project is to design and implement a vehicle that is powered by an electric motor, which in turn is energized using hybrid power with batteries. These batteries must have the capability to be recharged by a solar panel. A high-level block diagram, shown in Figure 1, outlines the major components that are necessary to control, power, and regulate the electric vehicle.

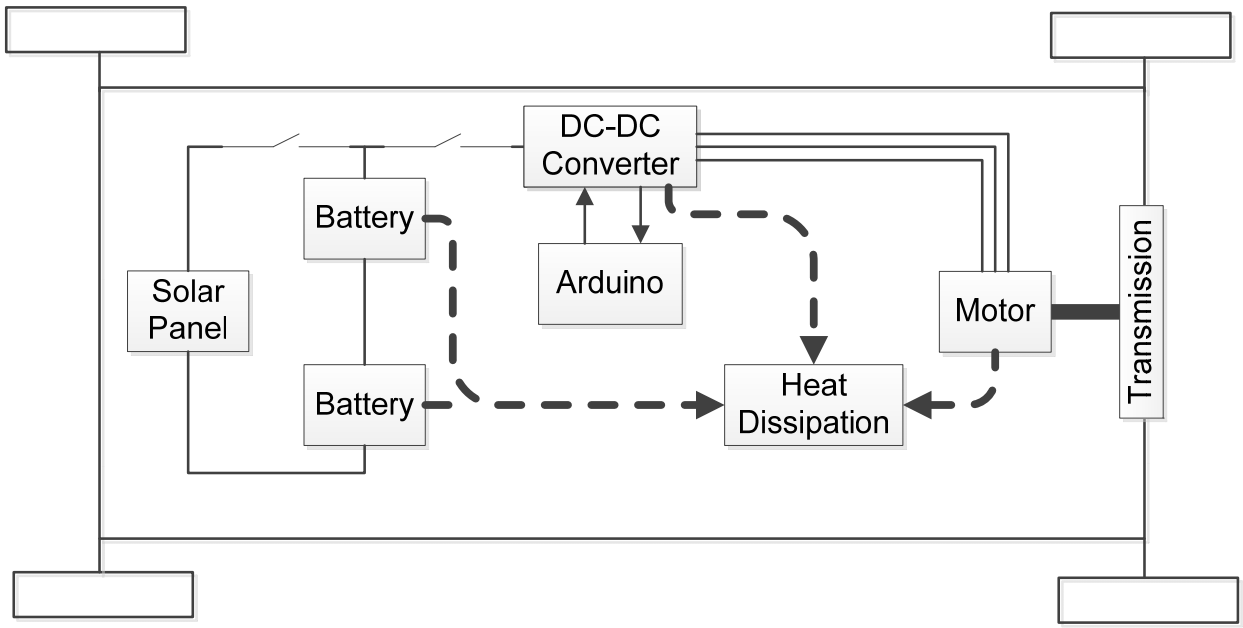

Figure 1: This is a high-level block diagram of the proposed electric vehicle.

To fulfill this goal, the design process should be guided by the main requirements and specifications, limitations, constraints, and directives delineated below.

Section 1.1: Requirements & Specifications

The following is a list of specifications that must be achieved in order to produce a successful, working vehicle.

- The batteries and DC motor must power and propel the vehicle. The batteries are responsible for energizing every part of the vehicle, and the DC motor is alone responsible for achieving locomotion.

- The solar panel must be able to recharge the batteries within 18 hours. The solar panel and a corresponding charging system will be used to charge the batteries when the system is not in use.

- The electric vehicle must be able to accelerate to a top speed of 7-10 mph in 15 seconds and maintain that speed for 60 minutes – this requires a constant motor torque of 3 N-m with a vehicle weight of 333 lbs., assuming a level asphalt road surface with no wind resistance.

- The vehicle must have an adjustable speed range in order to be practical. The vehicle should be able to function at speeds from 0 to 10 mph, depending on control from the driver.

- The efficiency of the electric vehicle should be at least 65%.

- The vehicle must have a cooling system sufficient to prevent any component from overheating. The cooling system should keep all components under their respective thermal ratings.

Section 1.2: Given Parameters

The design should employ the following fixed parameters to be successful.

- Two existing 12V UB12500 batteries should be used to power the vehicle.

- The battery-charging system should be driven by an existing Kyocera Photovoltaic Module, Model # KC85T.

- The vehicle should be propelled by an existing HPM5000B Brushless Motor made by Golden Motor.

- A complete simulation in Simulink must be created that accurately represents the vehicle.

- The weight of the electric vehicle, including the driver, must not exceed 400 lbs.

- The interface between the motor and the batteries should employ the DC-DC converter system produced by a previous senior design group. The existing converter is subject to burst noise and mechanical connection failure, and this must be addressed.

- The vehicle should employ the Baja chassis used by a previous senior design group, as well as its corresponding wheels and suspension system.

Section 1.3: Design Variables

The design variables may be adjusted throughout the design process in order to achieve a successful result. While there are a staggering number of variables in any engineering project, there are only a limited number of major design choices. The success of the final design will depend primarily on how well each of the following components are chosen or designed.

Hardware

- Control System/Interface – The vehicle needs to contain a controller that allows for the adjustment of motor speed/torque based on direct user control. The controller will also allow for braking and reverse modes.

- DC-DC Converter – The motor and batteries should be interfaced using the DC-DC converter with bi-directional four quadrant topology.

- Display – The vehicle needs to have a display that shows the current speed of the motor, the power left within the batteries, and the temperatures of the engine and battery. If time permits, an approximate time of operation can be included.

- Motor Coupling – The motor must be coupled via a transmission system to the existing Baja chassis.

Operating Conditions

- Speed – The speed should vary according to user input; as the driver presses on the accelerator, more voltage will be supplied to the motor to increase speed.

- Forward and Reverse Mode–The system needs to be able to operate in forward and reverse modes based on the driver's selection.

Section 1.4: Limitations and Constraints

The vehicle must adhere to limitations and constraints. These bounds serve to limit the time and cost of the project and make sure that no aspect of the vehicle becomes unmanageable. These limitations keep the vehicle a foreseeable, practical, reality.

- Cost – Design costs must be less than or equal to $1,000.

- Size – The vehicle's size will be determined primarily by the existing Baja frame, although the interior dimensions of the vehicle (the driver cavity) must be appropriate for a driver to operate the vehicle with relative comfort. This means that the cooling system must not inhibit driver motions, body positioning, or field of view.

- Weight – The vehicle's weight will be primarily determined by existing components, including the frame, driver, motor, two batteries, and solar panel. However, this means that the coupling system that connects the motor to the vehicle, as well as the cooling system, must not be so heavy that the batteries and motor can no longer propel the vehicle according to specification.

- Time – The project needs to be completed by December 2015 with a final design completed by May 2015.

Section 1.5: Additional Considerations

Other significant factors also need to be taken into account in the vehicle design.

- Safety –The system will contain safety features to prevent injury from mechanical and electrical components. Safety features may be implemented for the electric motor, gear systems, transmission, solar panel, and batteries.

- The vehicle must comply with the appropriate IEEE electrical standards, including the IEEE Standard for Electronics Power Transformers, the IEEE Guide for the Application of Electric Motors, and the IEEE and IEC Photovoltaic Standards. In order for the vehicle to be relevant to society, its design must uphold approved standards which would make it suitable for a commercial environment.

- Accuracy –We need to take in to account that all of our measurements may not be completely ideal since components contain uncertainty.

Section II: Detailed Design

In order to implement the concepts chosen in the concept evaluation process, detailed calculations and a specific design plan are needed.

Section 2.1: Charging Subsystem

Solar Panel

The solar panel will be mounted on the top of the electric vehicle, which is a flat surface. This is ideal since there is nothing between the solar panel and the sun.

For maximum charging efficiency, the solar panel should perpendicularly face the sun. This tilt should be allowed to vary over the year. For instance, in Fort Wayne, IN, the ideal tilt is 72° in July but only 26° in December. Therefore, a hinged mechanism is needed that allows the solar panel to be manually rotated to these angles. The mechanism should also allow the solar panel to collapse to the horizontal position when it is not in use. Two heavy-duty hinges will be purchased from Menards at $2.91 for both hinges in order to facilitate the solar panel tilt.

Section 2.2: DC-DC Converter

Decoupling Capacitors

Decoupling all voltage sources within the DC-DC converter is necessary to improve its efficiency and potential output. Consulting and research yielded the size of capacitor to use for this application. All sources suggested large capacitors in the range of 5,000-10,000 microfarad capacitors. Additionally, it was advised that the capacitor voltage ratings be about 5 volts above the maximum expected circuit voltage to guard against failure. The three internal voltage sources being decoupled are 15, 9, and 5 V. Therefore, one 20V-rated capacitor and two 16V-rated capacitors are chosen at a total cost of $30.00.

Enclosure and Securing of MOSFET Board

The MOSFET board of the DC-DC converter will be placed in a conductive aluminum enclosure with vent holes (1) to protect the board from debris and (2) to protect the driver and other equipment on the electric vehicle from the potentially harmful switching noise produced by the MOSFET board. Additionally, in order to make the power wires from the MOSFET board to the motor as short as possible, the enclosure will be placed in the rear of the vehicle near the motor. However, the enclosure will not be placed immediately next to the motor in order to minimize interference between the motor and MOSFET board.

The enclosure will be made as small as possible to take up a minimum amount of space. To reduce weight and decrease cost, the enclosure will be constructed out of 0.02 inch thick aluminum sheets. The bottom of the enclosure will be 0.125 inches thick

to give it extra strength. The side corners will be rounded in order to increase the strength of the enclosure.

The size of the gap between the MOSFET board and the inside of the enclosure was determined by calculations involving the maximum voltage in the controller and the dielectric constant of air to prevent air-gap shorts. The calculation used in this process is called the Paschen curve calculation.

$$V_b = \frac{apd}{\ln(pd) + b}$$

V_b = breakdown voltage for arcing
a = Dielectric constant of air = 4.36 x 10^7 V/(Atm-m)
p = pressure of the air
d = distance between conductive surfaces
b = Additional constant for air = 12.8

Using this equation, given the 72 V maximum of the DC-DC converter, the minimum distance between our two systems is less than one millimeter. In order to ensure no shorting occurs, a distance of half of a centimeter will be left between the two surfaces. Nylon standoffs and nylon bolts will be used to secure the enclosure to the board. The enclosure will be attached to the frame using fence post brackets attached to square brackets on the enclosure. The bolts can either be attached with large rubber dampeners to reduce the vibration.

Section 4.3: Cooling Subsystem

The power supplied by the various sources of energy in the EV will not be 100 percent efficient; therefore, they will produce an excess amount of heat capable of becoming detrimental to the system. Upon identifying the batteries as a substancial source of heat, a cooling system was designed. The system consists of forced convection produced by fans flowing over fins attached to the battery leads.

The fins, or heatsinks, provide a larger surface area for heat to transfer from the battery to the surrounding air of a lower temperature through the processes of conduction and convection.

The total amount of heat generated by one battery will be 110 W at an operating temperature of 45 ℃. Before considering heat removal by the fins, the total amount of heat dissipation without fins was calculated. This included forced convection on the top, front, bottom, and sides of the battery as well as on the leads. In order to promote uniform flow across the batteries, a set of two batteries will be enclosed by a duct with two fans at the entrance. The cooling subsystem will have a total of two ducts containing two batteries each shown in Figure 2. The ducts in Table 1 had to be lightweight and capable of supporting 60 lbs. The fans in Table 2 were selected based on high flow rate and low cost. The flow rate required was achieved by purchasing two

fans of 252 cfm at only $40 each. It was more cost efficient to purchase two fans of lower flow rate compared to one fan at double the flow rate.

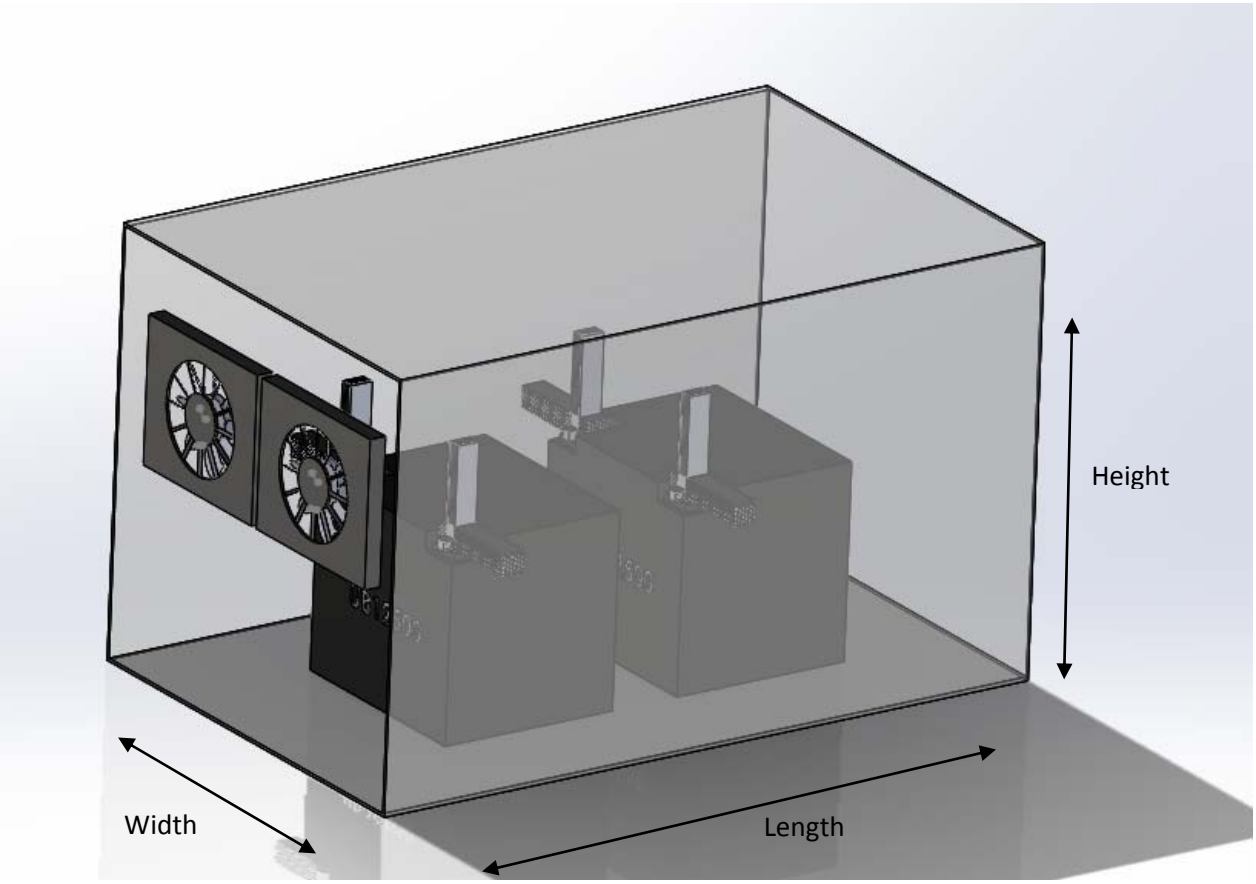

Figure 2: Cooling Subsystem Design

Table 1: Duct Dimensions & Specifications

Material	Steel CR Sheet
Thickness	.914 mm (.036 in)
Length	304.8 mm
Width	250 mm
Height	250 mm
Area	62500 mm^2
Weight	~ 10 lbs

Table 2: Fan Dimensions & Specifications

Model	Delta “Mega Fast”
Flow Rate (cfm)	252
Flow Rate (m^3/s)	.117
Dimensions	120 mm x 38 mm
Weight	< 5 lbs
Power Dissipation	48 W

The variables involved in the analysis and calculations of the cooling subsystem are listed in Table 3.

Table 3: Nomenclature

Variable	Descriptions	Units
V	Velocity of Air	$\frac{m}{s}$
$\dot{v}$	volumetric flow rate	$\frac{m^3}{s}$
A	area	m^2
A_c	cross sectional area	m^2
Pr	Prandtl number	unitless
a	battery length	m
L	Fin length	m
P	perimeter	m
Q	Heat transfer rate	W
$\bar{h}$	Convective heat transfer coefficient	$\frac{W}{m^2k}$
K	Thermal conductivity	$\frac{W}{mk}$
w	Width of the fin	m
R_c	Contact resistance	$\frac{m^2C}{kw}$
T_o	Base temperature	°C
T_∞	Ambient temperature	°C

In order to calculate the forced convection, the velocity of the air produced by the fans, V, was found using Equation 1 for volumetric flow rate; where $\dot{v}$ represents the volume of fluid that flows past a particular cross sectional area, A, per second. When solving for the velocity of air in the duct, the flow rate was doubled to account for two fans.

$$V = \frac{\dot{v}}{A} \qquad \textbf{Eq.1}$$

$$V = \frac{2 * .117\ m^3/s}{.0625\ m^2}$$

$$V = 3.744\ {}^{m}/_{s}$$

Next, thermal properties for the surrounding air at temperature T∞ were defined for the thermal conductivity, K, Prandl Number, Pr, and kinematic viscosity, v, in Table 4.

Table 4: Thermal Properties of Fin & Air

Air:	
T∞ (C)	20
K (W/mK)	.0257
Pr	.7088
v (m^2/s)	1.516 E -05

The flow was identified as turbulent or laminar for the sides of the battery using the Reynold's Number. The Reynold's Number in Equation 2 is the ratio of inertial to viscous forces of the flow. It was calculated using the velocity of air produced by the fans, the length of the side of the battery parallel to the flow, and the kinematic viscosity, v, of the air at T∞.

$$Re_a = \frac{V * a}{v} \qquad \textbf{Eq. 2}$$

$$Re_a = \frac{(3.744\ {}^{m}/_{s})*(.150\ m)}{(1.516\ x10^{-5}\ {}^{m^2}/_{s})}$$

$$Re_a = 37044.9$$

Since $Re_a < 5\ x10^5$ then the flow is laminar. Equation 3 is the average Nusselt Number correlation for forced convection with external parallel flow on a flat surface that is laminar.

$$\overline{Nu_a} = .664 * Pr^{\frac{1}{3}} * Re_x^{\frac{1}{2}} \qquad \textbf{Eq. 3}$$

$$\overline{Nu_a} = .664*(.7088)^{\frac{1}{3}}*(37044.9)^{\frac{1}{2}}$$

$$\overline{Nu_a} = 110.516$$

In order to calculate the heat transfer coefficient, the definition of the average Nusselt Number was used in Equation 4. The equation holds true for laminar flow, with a Pr ≥ 0.6.

$$\overline{Nu_a} = \frac{\bar{h} * a}{k} \qquad \textbf{Eq. 4}$$

$$110.516 = \frac{\bar{h}*(.15m)}{(.0257\frac{W}{mK})}$$

$$\bar{h} = 18.93 \frac{W}{m^2K}$$

The amount of heat removed by the parallel sides of the batteries was calculated using Equation 5 for heat transfer by convection. While the operating temperature was 45 ℃, T_o was defined as 40 ℃ to provide a factor of safety.

$$Q_{walls,\parallel} = \bar{h}A(T_o - T_\infty) \qquad \textbf{Eq. 5}$$

$$Q_{walls,\parallel} = \left(18.93 \frac{W}{m^2C}\right)(.0225\ m^2)(40\ ℃ - 20\ ℃)$$

$$Q_{walls,\parallel} = 8.519\ W$$

Next, the heat removed by forced convection on the perpendicular side, or front of the battery, was considered a non-circular body in laminar cross-flow with the Nusselt Number Correlation in Equation 6.

$$\overline{Nu_D} = CRe_D^m * P_r^{\frac{1}{3}} \qquad \textbf{Eq. 6}$$

The Reynold's Number in Equation 7 was based on an equivalent diameter, D, shown in Table 5 to be the height of the battery.

$$Re_D = \frac{V*D}{v} \qquad \textbf{Eq. 7}$$

$$Re_D = \frac{(3.744\ {}^{m}/_{s})*(.150\ m)}{(1.516\ x10^{-5}\ {}^{m^2}/_{s})}$$

$$Re_D = 37044.9$$

Table 5: Reynold's Number and Constants for Noncircular Cylinders

Geometry		Re_D	C	m
Square				
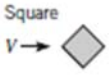		6000–60,000	0.304	0.59
		5000–60,000	0.158	0.66
Hexagon				
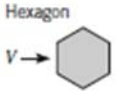		5200–20,400	0.164	0.638
		20,400–105,000	0.039	0.78
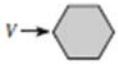		4500–90,700	0.150	0.638
Thin plate perpendicular to flow				
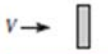	Front	10,000–50,000	0.667	0.500
	Back	7000–80,000	0.191	0.667

[a]These tabular values are based on the recommendations of Sparrow et al. [14] for air, with extension to other fluids through the $Pr^{1/3}$ dependence of Equation 7.52. A Prandtl number of $Pr = 0.7$ was assumed for the experimental results for air that are described in [14].

(From *Fundamentals of Heat and Mass Transfer*)

The values C = .158 and m = .66 were found for a cube using published experimental results in Table 5.

$$\overline{Nu_D} = (.158)*(37044.9)^{.66}.7088^{\frac{1}{3}}$$

$$\overline{Nu_D} = 145.946$$

In order to calculate the heat transfer coefficient, the definition of the average Nusselt Number was used in Equation 8. The equation holds true for laminar flow, with a Pr ≥ 0.6.

$$\overline{Nu_D} = \frac{\bar{h}*D}{k} \qquad \textbf{Eq. 8}$$

$$145.946 = \frac{\bar{h}*(.15m)}{(.0257\frac{W}{mK})}$$

$$\bar{h} = 25.005\ \frac{W}{m^2K}$$

The amount of heat removed by the perpendicular sides of the batteries was calculated using Equation 9 with the convective heat transfer coefficient.

$$Q_{walls,\perp} = \bar{h}A(T_o - T_\infty) \qquad \textbf{Eq. 9}$$

$$Q_{walls,\perp} = (25.005\ \frac{W}{m^2K})(.0225\ m^2)(40\ ℃ - 20\ ℃)$$

$$Q_{walls,\perp} = 11.252 \text{ W}$$

The total amount of heat removed by the walls of the battery by forced convection for four parallel sides and one perpendicular side was summed using Equation 10.

$$Q_{walls} = Q_{walls,\parallel} + Q_{walls,\perp} \qquad \textbf{Eq. 10}$$

$$Q_{walls} = 4*(8.519\ W) + 11.252 \text{ W}$$

$$Q_{walls} = 45.328 \text{ W}$$

The heat generated by the battery minus the heat loss through the sides will be removed by the fins on the battery leads (Equation 11).

$$Q_{fin} = Q_{gen} - Q_{walls} \qquad \textbf{Eq. 11}$$

$$Q_{fin} = 110 \text{ W} - 45.328 \text{ W}$$

$$Q_{fin} = 64.672 \text{ W}$$

In order to calculate the base temperature of the fins, the contact resistance between the battery lead and cap had to be analyzed. Since the battery lead and fin are composed of different materials with varying roughness, their surface areas do not touch entirely, and the heat dissipated by the battery is not fully transferred. As a result, the temperature at the base of the fin is less than the battery lead. The temperature at the base of the fin was calculated using the equation below for a contact resistance of 15×10^{-3} m^2C/kW. This was a worst case value based on experimental data found online. Equation 12 is based on two rectangular plane walls with one wall having a convective boundary condition. Part I of the equation represents conduction through the cap and the assumed contact resistance. Part II represents the convective boundary condition at the cap. Q_{lead} Represents the heat that will need removed by the fins per battery lead which is half the heat that needs removed from the entire battery by the fins.

$$Q_{lead} = \left(\frac{Q_{fin}}{2}\right) = \underbrace{\frac{T_1 - T_2}{\frac{L_2}{k_2 * A_1} + R_C}}_{\text{(Part I)}} + \underbrace{\frac{T_2 - T_\infty}{\frac{1}{h * A_2}}}_{\text{(Part II)}} \qquad \textbf{Eq. 12}$$

$$32.336 \text{ W} = \frac{(40\ ℃ - T_2)}{\frac{.002 \text{ m}}{\left(200 \frac{\text{W}}{\text{m K}}\right) * (.000731 \text{ m}^2)} + (15 \times 10^{-3} \text{ m}^2\text{C/kW})} + \frac{T_2 - 20\ ℃}{\frac{1}{\left(5.713 \frac{\text{W}}{\text{m}^2\text{K}}\right) * (.000867 \text{ m}^2)}}$$

$$T_2 = 39.13\ ℃$$

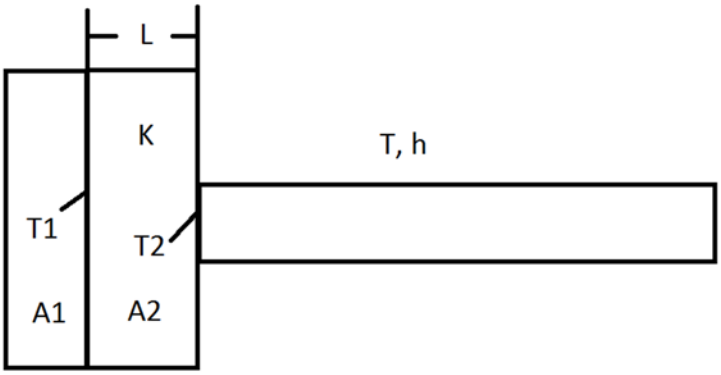

Figure 3: This is a thermal resistance and contact resistance diagram, where A1 is the area around the terminal and A2 is the area around the outside of the cap.

The width, thickness, and spacing of the fins were limited to the dimensions of the lead and were set to w = .019 m, t = .001 m, and s = .01 m respectively. The perimeter of the fin was P = .054 m; therefore, a total number of 27 fins was calculated using Equation 13 for each lead.

$$n = \frac{P}{(t + s)} \qquad \textbf{Eq. 13}$$

$$n = \frac{.054\ m}{(.001\ m + .001\ m)}$$

$$n = 27\ \text{fins}$$

The flow over the fins was identified as laminar by calculating the Reynold's Number with Equation 14 with respect to w as shown in Figure 4 and comparing it to $5\ x10^5$.

$$Re_w = \frac{V*w}{v} \qquad \textbf{Eq. 14}$$

$$Re_w = \frac{(3.744\ {}^{m}/_{s})*(.019\ m)}{(1.516\ x10^{-5}\ {}^{m^2}/_{s})}$$

$$Re_w = 4692.35$$

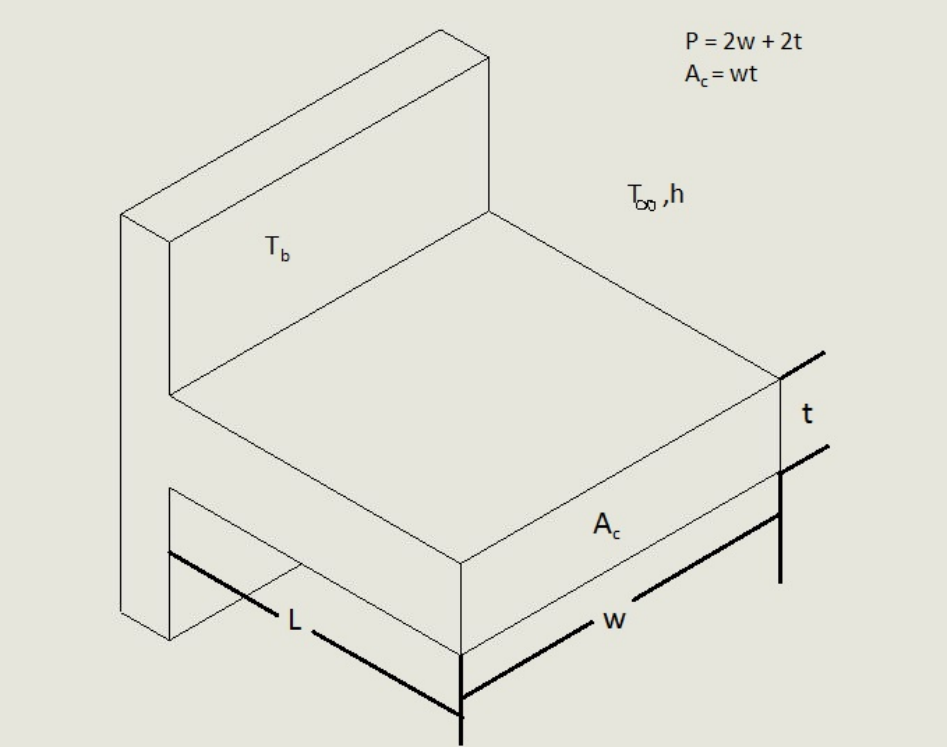

Figure 4: Fin diagram

Since $Re_X < 5\ x10^5$, the flow is laminar. Equation 15 is the average Nusselt Number correlation for forced convection with external parallel flow on a flat surface that is laminar.

$$\overline{Nu_x} = .664 * P_r^{\frac{1}{3}} * Re_w^{\frac{1}{2}} \qquad \textbf{Eq. 15}$$

$$\overline{Nu_x} = .664 * (.709)^{\frac{1}{3}} * (4692.350)^{\frac{1}{2}}$$

$$\overline{Nu_x} = 39.333$$

In order to calculate the heat transfer coefficient, the definition of the average Nusselt Number was used in Equation 16. The equation holds true for laminar flow, with a Pr ≥ 0.6.

$$\overline{Nu_x} = \frac{\bar{h} * w}{k} \qquad \textbf{Eq. 16}$$

$$39.333 = \frac{\bar{h} * (.019\ m)}{(.0257 \frac{W}{mK})}$$

$$\bar{h} = 53.199\ \frac{W}{m^2K}$$

Equation 17 solves for the heat transfer assuming a constant base temperature and convection at the tip of the fins where n is the number of fins at length, l.

$$Q = n * \sqrt{hPkA_c} * \theta_o * \frac{tanh(mL)+\frac{h}{km}}{1+\frac{h}{km}tanh(mL)} \qquad \textbf{Eq. 17}$$

The perimeter, cross sectional area, variable m, and temperature difference from Figure 3 were calculated in Equations 18, 19, 20, and 21 respectively.

$$P = 2w + 2t \qquad \textbf{Eq. 18}$$

$$P = 2 * (.019\,m) + 2 * (.001\,m)$$

$$P = .04\,m$$

$$A_c = wt \qquad \textbf{Eq. 19}$$

$$A_c = (.019\,m) * (.001\,m)$$

$$A_c = .000019\,m$$

$$m = \sqrt{{hP}/{kA_c}} \qquad \textbf{Eq. 20}$$

$$m = \sqrt{\frac{\left(53.199\ \frac{W}{m^2K}\right) * (.04\,m)}{\left(200\frac{W}{mK}\right) * (.000019\,m)}}$$

$$m = 23.664\ (\frac{1}{m})$$

$$\theta_o=(T_o-T_\infty) \qquad \textbf{Eq. 21}$$

$$\theta_o=(39.13\ ℃-20℃)$$

$$\theta_o=19.13\ ℃$$

For the ten inner fins, the length, l, is limited to .015 m. As a result, the heat removed by the inner fins, $Q_{fins,\ inner}$, is calculated for each battery lead using Equation 16.

$$Q_{fins,\ inner}=10*\sqrt{(53.199\ (\frac{W}{m^2K})*(.04\ m)*\left(200\frac{W}{mK}\right)*(.000019\ m)*(19.13\ ℃)*\frac{\tanh\left((23.664\ (\frac{1}{m}))*(.015m)\right)+\frac{(53.199\ \frac{W}{m^2K})}{(200\frac{W}{mK})*(23.664\ \left(\frac{1}{m}\right))}}{1+\frac{(53.199\ \frac{W}{m^2K})}{((200\frac{W}{mK})*(23.664\ \left(\frac{1}{m}\right))}\tanh((23.664\ \left(\frac{1}{m}\right)*(.015m)))}}$$

$$Q_{fins,\ inner}= 6.03\ W\ (per\ lead)$$

For the seventeen top and outter fins the required heat removal is equal to the total heat removal required by the fins minus the heat removed by the inner fins of both leads. This value is divided by two in order to analyze a single lead's heat transfer equation to find the required length,l, of the fins.

$$Q_{fins,\ outter}=\frac{Q_{fins}-(2*Q_{fins,\ inner})}{2} \qquad \textbf{Eq. 22}$$

$$Q_{fins,\ outter}=\frac{64.672\ W-(2*6.03\ W)}{2}$$

$$Q_{fins,\ outter}=26.306\ W$$

$$26.306\ W\ =17*\sqrt{(53.199\ (\frac{W}{m^2K})*(.04\ m)*\left(200\frac{W}{mK}\right)*(.000019\ m)*(19.13\ ℃)*\frac{\tanh\left((23.664\ (\frac{1}{m}))*L\right)+\frac{(53.199\ \frac{W}{m^2K})}{(200\frac{W}{mK})*(23.664\ \left(\frac{1}{m}\right))}}{1+\frac{(53.199\ \frac{W}{m^2K})}{((200\frac{W}{mK})*(23.664\ \left(\frac{1}{m}\right))}\tanh((23.664\ \left(\frac{1}{m}\right)*L))}}$$

$$26.306\,W\ = 17 * (.089924) * (19.13\ ℃) * \frac{tanh((23.664 * L) + .01124}{1 + .01124 * tanh((23.664\ * L))}$$

$$.89937\,W\ = \frac{tanh((23.664 * L) + .01124}{1 + .01124 * tanh((23.664\ * L))}$$

$$L = .0657\,m$$

The fin and cap apparatus will be machined from a solid block of 6063 Aluminum. Since the wire connection hole will be covered by the fin design, a new connection tab will be machined out of the Aluminum block with a hole of the same diameter. The design is shown in Figure 5 with dimensions in Table 6.

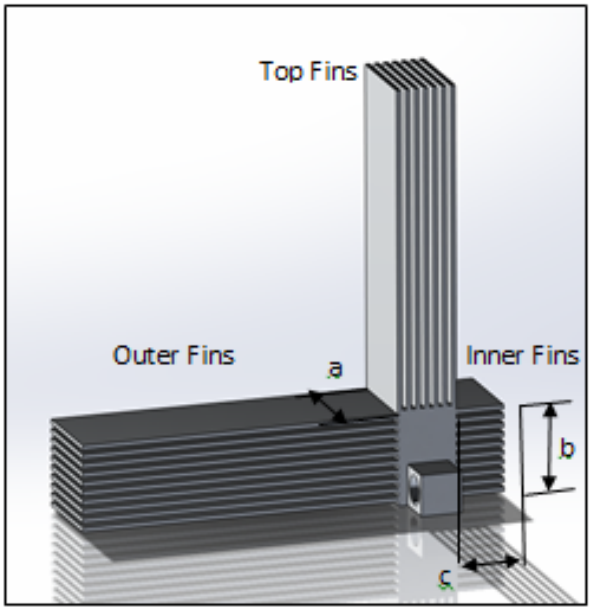

Figure 5: Fin design

Table 6: Fin Design Dimensions & Specifications

a	17 mm
b	17 mm
c	9 mm
L (outer fins)	70 mm
L (top fins)	70 mm
L (inner fins)	10.5 mm
w	19 mm
t	1 mm
Fin Spacing	1 mm
Number of Fins (Outer)	10
Number of Fins (Top)	7
Number of Fins (Inner)	10
Total Number of fins	27

A model of the fin was generated using SolidWorks according to the specified dimensions, material, base temperature, ambient temperature, and heat transfer coefficient in Figure 6. The simulation provided an estimate for the maximum length of the fins for which additional lengthening would not remove more heat since it is equal to the ambient temperature. This is equivalent to completing the Finite Difference Method where you can find the temperature at any point of the fin. This length was found to be 70 mm.

As the colors and corresponding scale on Figure 6 the tip of the fin is at 27 degrees Celsius, within 7 degrees of ambient. This was generated by applying a convective boundary condition to all sides and a constant temperature boundary condition on inside of the cap.

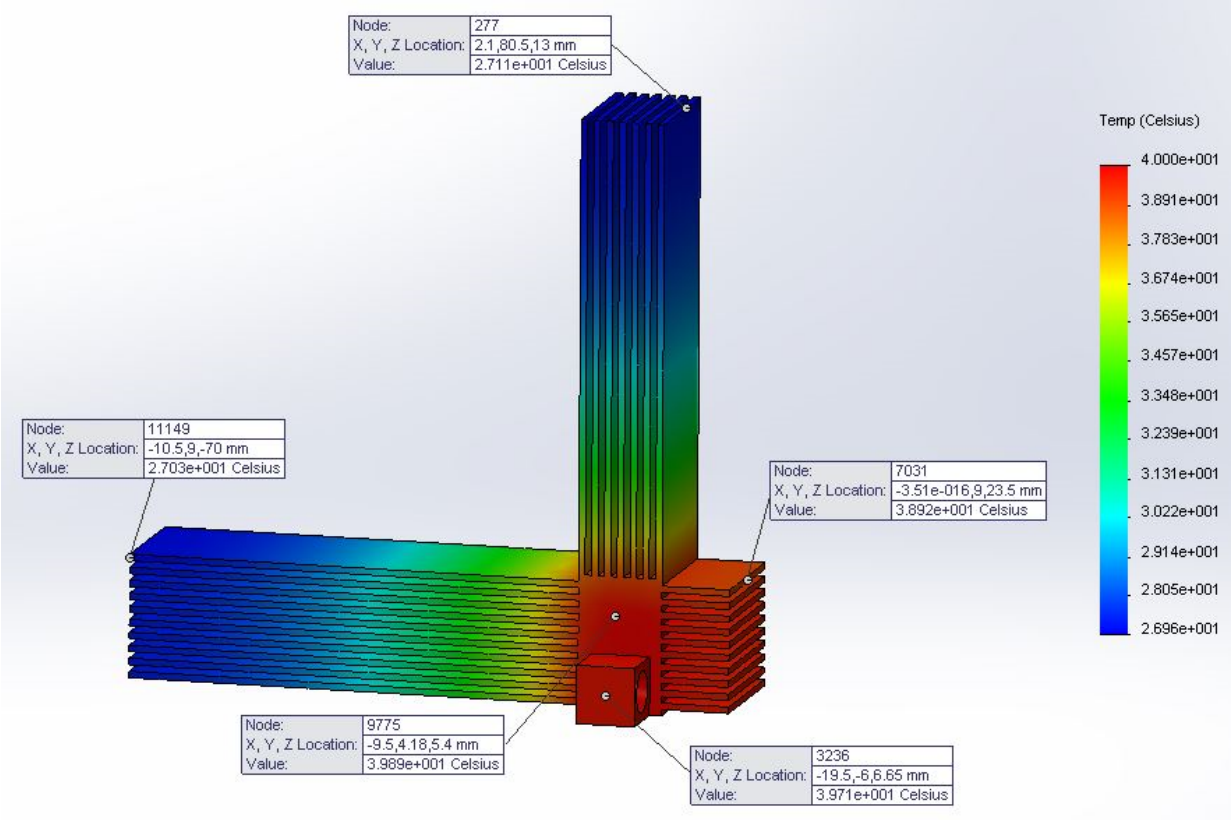

Figure 6: SolidWorks thermal study of the fin

A built-in simulation of SolidWorks estimated the cost per part for the fin design (Figure 7). The specified material properties and dimensions of the model estimated $98.83 to produce each fin. This estimate is rather high. A drawing for our fin design has been produced and will be submitted to a local manufacturing company for a quote. This will give us a better estimate of the cost to manufacture the fins, and will be much more accurate compared to the SolidWorks estimation.

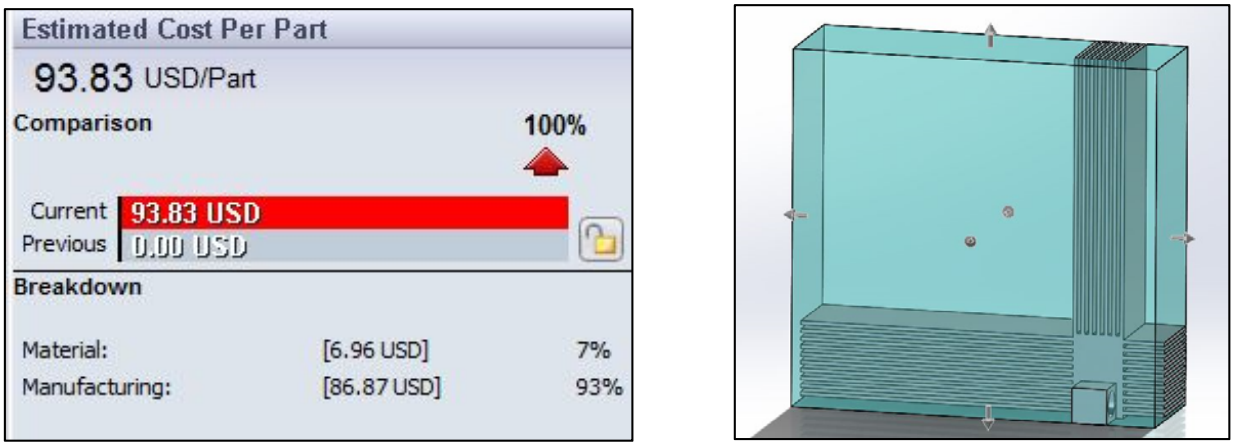

Figure 7: SolidWorks cost study of the fin

Section 2.4: Control Subsystem

A PID controller will be used to control the speed of the vehicle, which will be implemented using the Arduino. The system (Figure 8) consists of an input, an output, a plant, and a controller. The input of the system will be the code that is being sent from the rotary encoder. The output will be the voltage that needs to be sent to the motor. The plant of the system is the vehicle itself. As soon as it is operational, tests will be made to develop a transfer function that correctly expresses the speed of the vehicle related to voltage. Furthermore, there must be a controller that will modify the result to make sure that the resulting output is stable and helps the system perform at its optimum behavior.

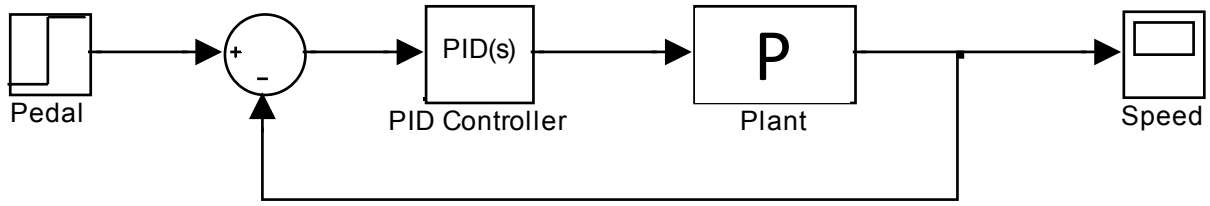

Figure 8: This is a Simulink model of the PID control system that will be used to control vehicle speed.

The cooling system will also be controlled by the Arduino. The cooling system will compare the current temperature in the sensors to a set constant (Figure 9). If the temperature is higher than the constant, the microcontroller will turn on the cooling system. The system will be kept cooler than 45°C, which corresponds to a TMP36 temperature sensor output of 0.950V. The system will not have a feedback loop since whether the cooling system is on or off will only depend on the current temperature on the sensors and not the output to the cooling system.

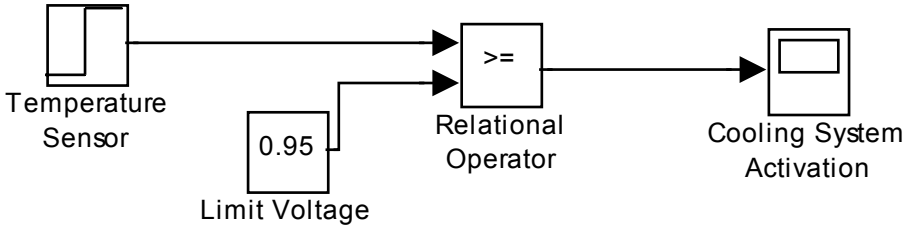

Figure 9: This is a Simulink model of the open-loop temperature control.

There is an existing shock control system that is already implemented in the mini Baja vehicle. This system consists of a controller (Figure 10) that receives inputs from each of the four shocks on the vehicle. The controller individually regulates the stiffness of each shock.

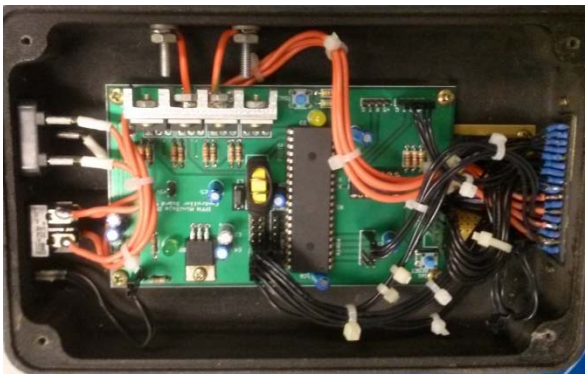

Figure 10: This is the shock controller that is already installed on the vehicle.

Arduino Capability

The existing microcontroller that is part of the existing DC-DC converter is the Arduino Mega 2560 (Figure 11). This microcontroller has 54 digital input/output pins (of which 15 can be used as PWM outputs), 16 analog inputs, and 4 UARTs (hardware serial ports). Only 6 analog inputs are currently being used, and there are more than a dozen digital inputs/outputs available. Consequently, the existing microcontroller should be able to handle the rotary encoder, the color LCD display, the temperature sensors, the speed sensor, and the stepper motor.

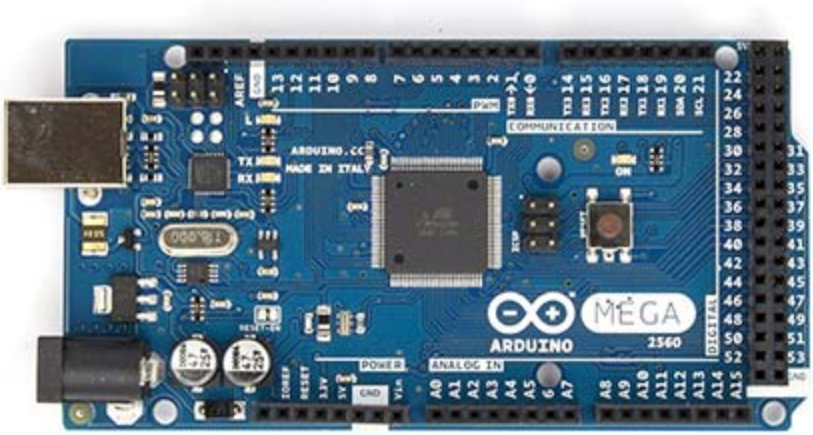

Figure 11: This is the Arduino Mega 2560 microcontroller currently in use in the DC-DC converter.

Rotary Encoder for Pedal

Currently, the motor speed is controlled by a potentiometer dial on the DC-DC converter control box. However, control of the motor must be transferred to the pedal of the electric vehicle. To accomplish this, a rotary encoder will be purchased to replace the rotary potentiometer that is currently on the system. Since a rotary encoder converts angular position of a shaft to a voltage signal, it is ideal for the rotational movement of the existing pedal.

In order for the user to be able to control the vehicle smoothly and naturally, it is determined that the error of the conversion of pedal movement to motor voltage should be no greater than 2%. Therefore, it was decided to purchase the 200 pulse-per-rotation A2A6 CWZ 6C rotary encoder (Figure 12). This will result in a 0.5% resolution for the pedal-to-voltage conversion, four times better than specification.

Figure 12: This is the rotary encoder that will be used to read the rotational movement of the existing pedal.

This rotary encoder has been chosen because there are existing projects using this encoder with an Arduino microcontroller. These projects ensure that the encoder will work with the existing Arduino microcontroller and can also be used as a reference when programming the rotary encoder into the existing codebase. The price of the encoder is $39.95.

LCD Display

A new LCD screen is needed because the one currently connected to the Arduino is not large enough to display the necessary information. The information that the LCD should display includes vehicle speed, battery temperature, battery voltage, remaining battery life, various warnings (e.g., 1 yr. to replace batteries, current limit reached, etc.), battery current, and ambient temperature. Furthermore, a color LCD is needed since color LCDs are more user-friendly than monochrome displays, and with the wealth of information to display, the information should be as easy as possible to grasp. When all these requirements are taken into account, the SSD1963 Color 8" TFT Touch Shield LCD Display Module for Arduino (Figure 13) is chosen as the best LCD display. This screen is ideal because its main purpose is to interface with an Arduino microcontroller, so consequently there are existing sample codes that can used as a reference when creating the LCD code for the microcontroller. The cost of the LCD screen is $52.19. It is also recommended to buy a protector, since the LCD is meant for outdoor use. The cost of this protector is $7.79. This makes the total cost of the LCD screen with protector $59.98, plus taxes and shipping.

Figure 13: This is the 8” LCD display that will be installed in the electric vehicle.

Temperature Sensors

The TMP36 analog temperature sensor (Figure 14) is a time-tested, rugged IC chip. It can be used for both temperature-sensing applications – battery temperature and ambient (environment) temperature. An epoxy glue can be used to securely attach the temperature-sensing chip to each of the batteries as well as an external part of the vehicle. They are $1.50 each, so if one is purchased for each battery, and one is purchased for the ambient temperature, the total cost would be $7.50 plus shipping and tax.

Figure 14: This is a TMP36 analog temperature sensor; it will be used to measure the battery and ambient temperature on the vehicle.

Speed Sensor

For proper system control, as well as for the driver’s sake, it is important to detect the exact speed of the vehicle. This can be accomplished by tracking the number of rotations of a vehicle axle. One of the simplest and most rugged ways to measure axle rotation is to create an iron-cored coil with a magnet attached to one end. When ferrous metal is moved near this coil, a current is induced in the coil due to the changing magnetic field in the coil. By fixing the coil near the teeth of a rotating gear, the

rotational speed of the gear can be determined by measuring the frequency of the sinusoidal waveform produced in the coil.

An Instructables.com user named Peter has documented a means to create such a magnetic sensor. The following procedure is a modification of Peter's method that is feasible for this team. Magnet wire, which is copper wire with a very thin insulating layer to allow for more turns in a given volume, can be coiled around a small iron core many times to create an iron-cored coil. This can be slipped inside a thin insulating wrapping, and the entire device slipped inside a hollowed-out large bolt. Epoxy or hot glue can be used to solidify the coil inside the bolt. A small magnet is placed on one end of the bolt – preferably the head, where the two leads from the two ends of the coil are protruding from the bolt. The other end of the bolt can be fixed within a few millimeters of the teeth of a gear attached to the axle. Such a configuration is a very durable, reliable, dirt-immune speed sensor similar to those used for ABS in many automobiles.

For $7.19, ample lengths of 22, 26, and 30-guage (AWG) wire can be bought. These correspond to 0.64mm, 0.40mm, and 0.25mm wire diameters respectively. A pair of small rare earth magnets (3/16" diameter) can be purchased for $0.43. By interfacing leads from the two ends of the coil of wire with the microcontroller, the speed can be easily calculated.

Stepper Motor for Cruise Control

When the vehicle cruise control is activated, the electric vehicle should maintain its current speed without needing the driver to continue pressing the pedal. The pedal should maintain the position it had prior to activation of cruise control. Consequently, a stepper motor is needed to prevent the pedal from moving when cruise control is being used. The maximum amount of torque necessary to depress and hold the pedal is approximated to be no more than 50 lbs. at a distance of six inches. This translates to a torque of 100 foot-pounds. Using this parameter, a ROB - 09238ST stepper motor (Figure 15) is selected, as it has a holding torque of approximately 150 lb/ft, which is ample.

Figure 15: This is a strong stepper motor that will be used to control the pedal when the vehicle is operating on cruise control.

Section III: Design Modifications

The design underwent several changes as the building of the electric vehicle progressed.

The most significant design change was the replacement of the DC-DC converter/motor controller. The DC-DC converter/motor controller originally intended for the electric vehicle did not operate as designed and sustained damage upon attempts to repair it. Consequently, an alternate motor controller, the MBL1660N, was purchased. The new motor controller can handle up to 60 V and 120 A, exceeding the specifications of the original motor controller. The MBL1660N has advanced software controlling, moderating, and regulating its output voltage and current. Several safety features were preprogrammed into the controller, including overcurrent protection, overvoltage protection, customizable voltage and current limits, and motor trouble handling routines. (For example, if the controller detects that the motor is not moving but is receiving power, it will shut down to prevent damage to the motor.) The motor controller receives this information via the Hall sensor outputs from the motor.

The purchased motor controller was used to implement control for vehicle speed in place of the Arduino.

The cooling system is controlled by a manual switch, rather than a temperature sensor. As temperatures did not rise as radically as anticipated, it was convenient to be able to control the fans at will rather than limiting their operation time to a particular temperature range.

The shock control system was not activated. As the locality of testing was intended to be smooth asphalt or concrete, there was no need for the advanced controls available in the shock control system.

The specified color pixel-based LCD screen was purchased but not implemented. The display is of a very advanced nature; more than 40 hours of time was spent attempting to make the LCD operational with the Arduino Mega 2560. The absence of manufacturer-supplied code examples combined with the LCD being an unusual one resulted in a failure to make it operational. As a result, a simple four-line character-based LCD was purchased instead. This display proved sufficient.

The designed speed sensor used current induced by a changing magnetic field to measure the vehicle speed. A magnet was to be fixed on the end of an iron core, around which several turns of magnet wire were to be wrapped. As the teeth of an iron sprocket in the vehicle transmission neared and left the tip of the speed sensor, current would be induced in the turns of wire due to the presence of the magnetic field produced by the fixed magnet.

However, this design proved insufficient because the amplitude of the current spikes produced by the sensor was far too small to measure. In addition, the tip of the iron core had to be placed less than a millimeter from the sprocket to achieve appreciable results. Consequently, an alternate design was chosen – the reed switch and magnet.

A tiny magnet is fixed to the vehicle sprocket, and a reed switch placed within two centimeters of the sprocket. When the magnet passes near the reed switch, it pulls the iron switch in the reed switch closed, completing a circuit, and when the magnet leaves, carried away by the rotation of the sprocket, the reed switch opens again. This voltage signal can be easily measured by the Arduino, and proved a very reliable speed measurement method, as can be seen in the speed sensor testing results.

The design of the cruise control system was expanded and completed; its derivation can be found in Appendix A. Cruise control was not implemented due to time constraints.

Section IV: Build Process

Section 4.1: Speed Sensor

A reed switch, resistor, and magnet were hardware components required by the Arduino microcontroller to program the speed of the electric vehicle. The assembly works as a proximity sensor where the switch detected the target position of the wheel where the magnet is mounted. Upon actuation by the magnetic field, contact is made between the internal metal reeds of the switch. As a result, a closed circuit is produced. A resistor was soldered in series with the reed switch, and the output of the system was connected between both components. The idea of this is to obtain the voltage across the resistor. The normally open reed switch provides a zero voltage drop across the resistor while the actuated, closed reed switch permits a proportional voltage drop across the resistor. In a closed circuit, most of the voltage drop occurs across the resistor due to its higher resistance.

The reed switch and resistor assembly was securely mounted in a fixed location on the frame of the vehicle using an aluminum bar. The assembly was installed within close proximity of the path of the magnet traveling within the plane of the rotating sprocket. The magnet was also secured to the sprocket in a manner that prevented movement. The prevention of unintended movement was necessary in order to provide a reliable and consistent reading to the Arduino. Details on the programing of the speed sensor are explained in section 4.3.

Section 4.2: LCD

The configuration of the LCD display was one of the more time consuming challenges faced by the electronic group. An 8-inch display with 40 pins was originally purchased to provide an optimal display to the user. Unfortunately, the code provided by the manufacturer was not compatible with the EV system. Despite several attempts to work with the manufacturer to troubleshoot the system, a resolution was never achieved. Various forums related to the Arduino were researched, and a TFT library recommended as a possible solution did not resolve the issue. Additional troubleshooting included variations in code, modification to the manufacturer's code, checked connections, and cable reconnections. Resolution was never achieved with the original display, and the team implemented a less complex display due to the time constraint.

The less complex display was chosen due to component familiarity as it had been used in previous school related projects. If required, assistance would be available within the IPFW Engineering Department, eliminating manufacturer dependence. The display selected contains 16 pins: 1 source, 1 ground, 1 backlight source, 1 backlight ground, 1 enabler, 1 read/write, 1 data/command, 1 contrast, 4 data pins, and 4 pins not in use. The two grounds, the contrast, and the enabler were connected to the common ground pin of the Arduino. The two sources were connected to the common 5V pin from the Arduino. The 4 data pins, the read/write pin and the data/command pin were connected to their respective pins on the Arduino

Section 4.3: Programming of the Arduino

A code was created and uploaded to the Arduino microcontroller to interface all of the components within the EV system. The Arduino was designed to control the LCD screen display and the DC-DC converter using the inputs from the pedal, the temperature sensor, and the speed sensor. All of the pins used in the code were declared as constant integers on the code which can be found in Appendix D. Protected wires were used to transmit electrical signals from various components of the vehicle to the Arduino. The Arduino and its connections for 5V sources and ground were securely mounted to the EV using a Plexiglas box to protect the delicate hardware from outside contaminants. Fabrication for the box consisted of dimensioning and cutting five Plexiglas panels fastened using aluminum angle, screw, and nuts.

The encoder is a relative encoder; therefore, every time the system is rebooted (turned OFF and ON) the initial point for the encoder will be set at the current position of the encoder upon system activation. The code reads the input from the encoder by comparing the two signals sent from the encoder, A and B. The following scenarios describe the reaction to the signals:

- If A and B are the same, the encoder is not moving and the pulse count will stay the same
- If A is higher than B, the program will increase the pulse count
- If B is higher than A, the program will decrease the pulse count

When calibrating the system, the range was set between 0 and 672 pulses. The pulse output of the Arduino works with a duty cycle that can be determined by a value from 0 to 255. As a result, a linear relationship was established between the pulse count and the pulse output for the controller. A pulse output was chosen over analog output due to the analog outputting a significant amount of noise during testing. For preventative purposes, a safety mechanism was placed on the code. This mechanism will prevent the output from going outside of the 0 to 255 range in the event of the pulses somehow changing.

The speed sensor is composed of a resistor and reed switch assembly fixed to the EV frame and a magnet mounted on the sprocket. Every time the sprocket completes a full rotation, the magnet will pass through the reed switch, sending a pulse to the Arduino. When the Arduino receives this pulse, it will cause and interrupt and it will divide the circumference of the wheel (distance the car has traveled) by the time elapsed since the last pulse. The program measures elapsed time by resetting the timer upon receipt of each pulse. Due to the relatively low speed of the EV, the program required the addition of a variable to prevent the Arduino from reading the speed sensor more than once per revolution due to the length of time it takes for the magnet to clear the reed switch. This was accomplished through the use of a state variable that requires the state of the magnet to change from “closed” to “open” prior to accepting another pulse.

Only one temperature sensor was included in the current code of the EV. This temperature sensor collects the ambient temperature using a TMP 36. TMP36 functions by assigning a certain mV output to 25 degree Celsius and adding or subtracting 10 mV for every degree addition or subtraction respectively. The analog input of the Arduino accepts a value between 0 and 5 V and converts it to a digital value between 0 and 1023, giving it a resolution of 4.9 mV per bit. Once the relationship between voltage and temperature described above is obtained, the microcontroller converts the temperature from Celsius to Fahrenheit.

The less complex display was coded using the LiquidCrystal library from Arduino. The library includes various functions and commands that can be implemented to simplify the commands on the screen.

Section 4.4: Vehicle Wiring

Due to the large variety of electronic components within the vehicle, it was necessary to install a large amount of wiring in the vehicle. A 24 gauge wire from Ethernet cable was used to connect the LCD and digital encoder (both mounted in the front of the vehicle) to the Arduino and motor controller (mounted in the rear of the vehicle). In addition, an 18 gauge wire was used to connect a switch in the front of the vehicle with the motor controller. This wiring was enclosed in protective plastic tubing and fastened close to the longitudinal frame of the vehicle to ensure that the wiring was not disturbed by vehicle use.

In the rear of the vehicle, the batteries were connected to the motor controller via 6 gauge wire for operability at high DC current. In line with the batteries is a 120A fuse (installed on the recommendation of the motor controller literature) and a breaker (for safety purposes), which can be switched on and off manually. The three motor phases, as well as the motor hall sensors, were connected to the motor controller via a 10 gauge wire, which is the maximum size the motor controller can support. The Arduino was also connected to the motor controller via 24 gauge wire for pedal input. A speed sensor fastened near the right rear axle was connected to the Arduino for speed measurement.

Section 4.5: Solar Panel Mount

The solar panel was securely fixed to the top of the vehicle using purely a non-permanent method of attachment. The method of attachment to the top of the vehicle frame was to lay three flat pieces of metal laterally across the top of the vehicle, and secure each of them with an adjustable metal clamp. This has the benefit of not compromising the structural integrity of the vehicle frame. Two rectangular hinges were used to fix a short end of the solar panel to the rearmost lateral bar. Across the foremost two lateral bars, another flat metal piece was fixed perpendicularly, and three notches cut out of it. Then a hinged bar was bolted to the solar panel near the opposite end, so that the bar may swing into the notches cut in the bar fixed below it. In this

manner, four possible angles of rest – 45 degrees, 30 degrees, 20 degrees, and 0 degrees (flat) are obtained.

Section 4.6: Motor Controller

The DC-DC converter/motor controller originally intended for the electric vehicle did not operate as designed and sustained damage upon attempts to repair it. Consequently, an alternate motor controller, the MBL1660N, was purchased. The new motor controller can handle up to 60 V and 120 A, exceeding the specifications of the original motor controller. The MBL1660N has advanced software controlling, moderating, and regulating its output voltage and current. Several safety features were coded into the controller, including overcurrent protection, overvoltage protection, customizable voltage and current limits, and motor trouble handling routines. (For example, if the controller detects that the motor is not moving but is receiving power, it will shut down to prevent damage to the motor.) The motor controller receives this information via the Hall sensor outputs from the motor.

Interestingly, motor controller phase outputs and Hall sensor inputs are not standardized with motor phase inputs and Hall sensor outputs. For this reason, 36 phase/Hall sensor configurations are possible, and required testing in order to determine the correct connection profile. The 36 possible configurations were listed and then tested one by one at low voltage and current. This was done by connecting the Hall sensors and motor phases in a particular configuration, and then attempting to command the motor to rotate. If either no motion or high current with no motion was detected, another configuration was tested. The correct configuration was found after less than a dozen configurations were tested, and is shown in Table 7.

Phase Connections	
Motor	**Controller**
Green	U
Blue	V
Yellow	W
Hall Sensors	
Motor	**Controller**
Red	Top of Connector
Black	--
Green	--
Yellow	--
Blue	Bottom of Connector

Table 7: Motor-Controller Phase & Hall Sensor Connections

Besides the Hall sensors and the motor phases, the motor controller required a supply voltage and an ON/OFF voltage control. The supply voltage was initially supplied by a low-power DC power supply with a maximum of 20 V and about 2.1 A for safety purposes during testing. When the correct motor configuration was determined, 12 V

sealed lead-acid batteries were connected in series to the motor controller voltage input connections. However, the motor controller also uses a PWR CTRL connection for it on and off states. This, as discussed before, was wired to the front of the vehicle and back, and was alternately connected to the voltage supply and ground, depending on whether the vehicle should be on or off, respectively.

The motor controller also sports a serial interface that can be used to connect to a PC running specialized software designed to allow the PC user to configure motor controller settings. The final motor controller settings are captured in Appendix C.

The same serial interface that can be used to connect the motor controller to a PC was designed to receive a variety of control signals for the motor speed, including analog and pulse (digital) signals. The pulse signal from the encoder was routed to the motor controller via this interface (although first passing through the Arduino to record the magnitude of the pedal press.

Instructions were created to make sure that the vehicle is turned on and off properly by future users. In Appendix B, step-by-step instructions can be found on how to turn on the vehicle and how to turn it off. This document also includes preventive checks that should be done to make sure that none of the components get damaged.

Section 4.7: Motor Mount

The purpose of the motor mount was to provide a sustainable method for keeping the motor in the proper position for the CVT transmission. The motor mount itself was designed to withstand the maximum shear stress possible due to the maximum torque that the motor will produce. The mount frame contains slotted bolt holes for adjustability when it is mounted to the frame of the vehicle. The adjustability that comes with slotted holes gives three degrees of freedom for the motor to move and provide the transmission with optimal belt tension. The mounting process is simple and only uses four standard bolts through the frame and four standard bolts through the front of the electric motor.

Section 4.8: Motor-CVT Coupling

During the build process of the electric vehicle, the method of coupling the motor to CVT was very important related to the reduction of vibration and adapting a CVT transmission to convert the rotary motion of an electric motor to the wheels. The motor coupling uses two different sleeve shaft couplers. The first coupler was attached directly to the motor shaft and has the sole purpose of increasing the shaft diameter to 1 inch. Increasing the shaft diameter made extending the motor shaft to the appropriate length possible by adding an additional standard 1 inch shaft. The 1 inch shaft reducer coupling was coupled using an equivalent diameter sleeve coupled to the extended shaft. With the desired length of the shaft acquired, the top pulley of the CVT was then fit to the end of the shaft. All of the couplers were keyed in order to prevent slipping within the coupling sleeves.

Section 4.9: CVT Modification

In order for the existing CVT designed for the previous combustion motor to work with the electric motor, it had to be modified for a lower rpm range. This was accomplished by disassembling the top pulley of the CVT and disconnecting the springs attached to the centrifugal weights. This enabled the CVT to operate at the current lower RPMs due to the reduction in force in order to move the centrifugal weights.

It was also necessary to cause the CVT to be constantly engaged. This was achieved by inserting four washers on the bolts to act as spacers attached to the centrifugal weights, thereby reducing the distance the pulley can extend. This closed the top pulley enough that it was always in contact with the belt. This was necessary due to the fact that the CVT was originally designed to have a range of RPMs at which the system would idle. After passing through this range, the CVT would then engage. By forcing the CVT to be engaged, the RPM requirements of the CVT were further decreased.

Section 4.10: Fin Construction and Mounting

The mechanical group received a quote from an outside vendor to fabricate the fins which greatly exceeded the project budget at approximately $800.00. As a result, the fins were machined by the IPFW machine shop out of a square 6061 aluminum bar. This method involved long lead times; therefore, the materials were materials were ordered and provided to the machine shop during the summer prior to Fall Semester. After the fins were machined, holes were drilled and tapped to accommodate the mounting screw and thermocouples. The mounting screw was added to the fin design after it was determined that a press fit would not be sufficient in holding the fins on the battery terminals. The fins were machined slightly out of tolerance; therefore, their installation required a hammer to overcome the force of the terminals. Once the fins were hammered to the base of the terminals, they were removed. Thermal compound was applied to the terminals to ensure all air gaps were filled. After the fins were replaced on the terminal, the mounting screws were inserted until they pressed tightly against the terminals. This method firmly mounted the fins to the battery terminals and ensured optimal terminal to fin contact on at least three sides.

Section 4.11: Fans

Plexi-glass was cut to size and mounted to the frame of the vehicle surrounding the battery mounting system. Fans powered by the batteries were mounted to the glass with screws included by the manufacturer, and provide forced convective heat transfer on the fins. The configuration shown in Figure 16 provides one fan directly aimed at each heat sink.

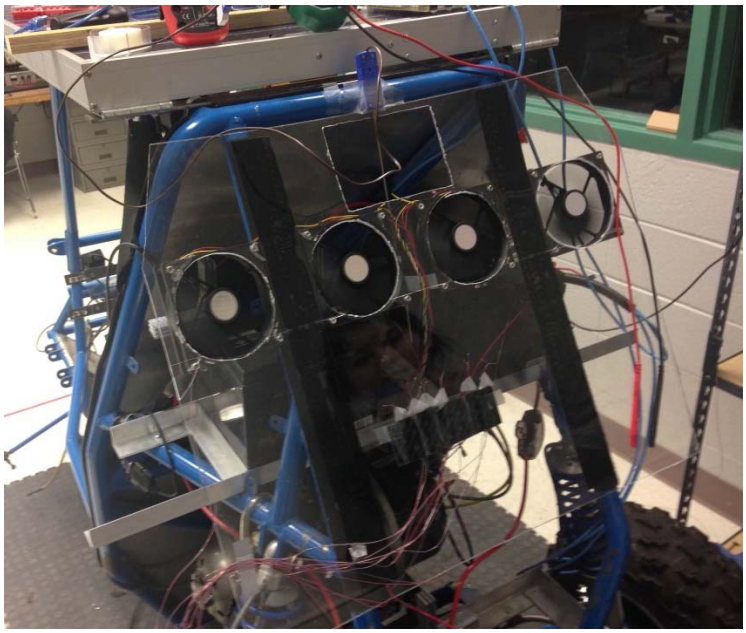

Figure 16: Mounted Fin Assembly

The sheets of plexi-glass were velcroed onto the back of the vehicle for convenient removal. The fans' electrical connections were made in parallel; and the entire system pulls 9 volts from the upper, left battery.

Section 4.12: Pedal and Encoder

The accelerator pedal of the fuel injected system was repurposed during the conversion to an electrically powered vehicle. The system required modifications following the removal of the throttling system in order to mechanically return the pedal to its standby position following the discharge of driver input and electrically send a response to the main system dependent upon driver input.

The existing gas pedal returned to the standby position using the internal spring of the throttle linkage. The component was replaced with a tension spring interconnecting the pedal and the frame of the vehicle. A spring stiffness was selected large enough to return the pedal to the start position yet small to not cause fatigue to the driver due to a large opposing force.

An encoder was implemented to create an electrical response to the main system dependent upon the driver's input to the accelerator pedal. A pinion was coupled with the shaft of the encoder, and the system was mounted in line with a corresponding rack fastened to the accelerator pedal. The rack was positioned below the pinion, and constant contact between the components was achieved using a tension spring applying an upward force on the rack. The linear displacement of the pedal and rack of the user causes the shaft of the encoder to rotate with the coupled pinion. As a result, a programmable relationship for speed and user input was achieved.

Section 4.13: Batteries

The EV system is capable of handling five 12 V batteries, and accommodations for four were made. The batteries are supported by aluminum angle mounted directly to the rear of the frame with (diameter here) steel nuts and bolts. The angled design prevents the batteries from moving in the horizontal directions while Velcro straps prevent them from lifting off of the moving vehicle. Two batteries were mounted toward the top of the vehicle and accommodations for two more were made next to the motor.

Section V: Testing

Section 5.1: Solar Charging System Testing

The solar panel was tested by connecting the solar panel to two discharged batteries. The two batteries were discharged by connecting them individually to a car in place of the standard battery and running the lights and fans until the battery could not support running these systems any longer. Once the batteries were discharged, they were connected in series to the solar panel. This system was then placed outside in the sun for several days, during which the voltage across the batteries was measured periodically (Figure 17). When it increased rapidly, the batteries were disconnected. One of the batteries was then attached to the car and the discharge time was compared to the original time to check if the batteries were fully charged.

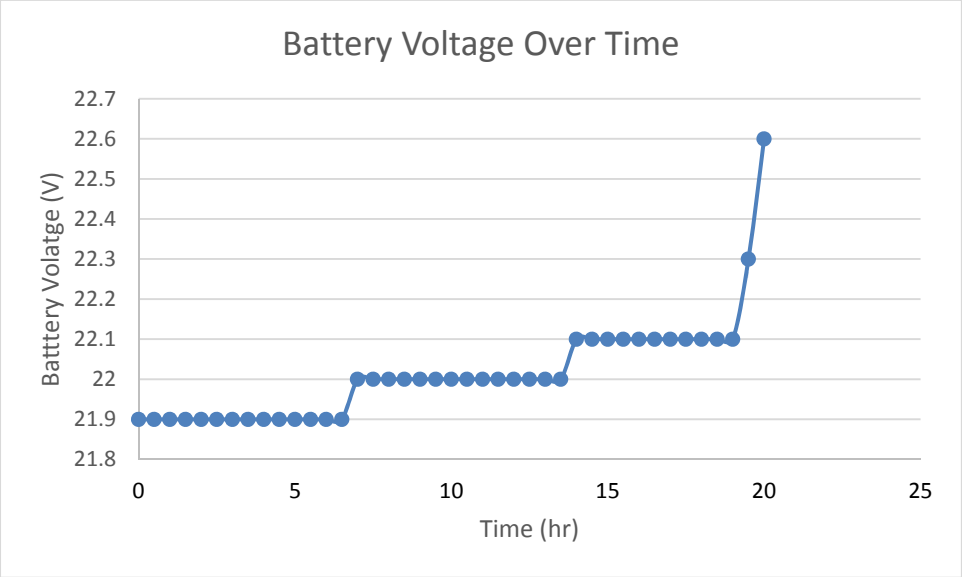

Figure 17: The measured voltage across two batteries during charging with the solar panel.

As evident in Figure 17, the measured charging time for this testing was 20 hours.

Section 5.2: Speed Sensor Accuracy Testing

The speed sensor was tested for accuracy against a calibrated device. A laser tachometer was used to measure the rotational speed of the wheels, and these values were then multiplied by a transformation ratio to convert the wheel rotation speed to linear speed. The circumference of the wheels was measured to be 5.64 feet, so rotations per minute can be converted to miles per hour using Equation 23.

$$\frac{rotations}{minute} \times \frac{5.64\ feet}{rotation} \times \frac{60\ minutes}{hour} \times \frac{mile}{5{,}280\ feet} = \frac{miles}{hour} \qquad \text{Eq. 23}$$

Under no-load conditions, the vehicle was run through the entire speed range at periodic intervals of the motor controller command values. These values were modified

with serial commands from a computer. The speed sensor displayed the linear speed to the LCD screen while the tachometer reading was recorded separately. These two values were then compared using the magnitude of the difference between them. This comparison is shown in Figure 18.

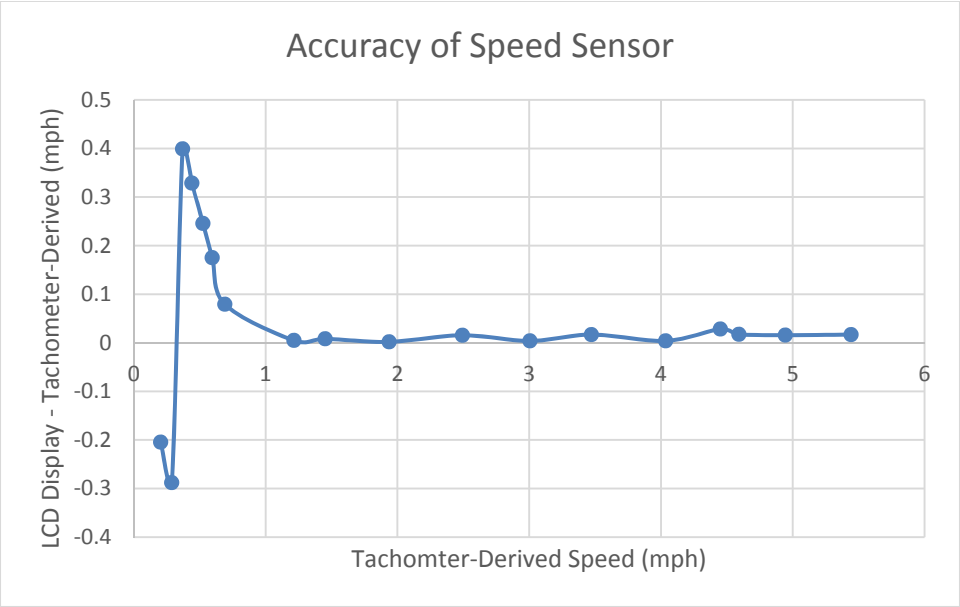

Figure 18: Precision of the speed sensor compared to the calculated value from the tachometer

As the figure shows, the speed sensor has its worst precision at speeds of less than one mile per hour. This is a result of the speed sensor being designed to handle higher speeds. Once the speed is greater than one mile per hour, the difference between the sensor on the car and calculated value from the tachometer becomes less than 0.05 miles per hour.

Section 5.3: System Dynamic Power Testing (No Load)

Running the system through the speed range shows how the speed of the vehicle can be related to power that the system draws. This relationship can be used to predict the performance of the system in the future. For the test, the controller was receiving command values serially through a computer. The power was measured by reading the voltage and current from a multimeter connected across and in line with the batteries. The results are shown in Figure 19 and Figure 20.

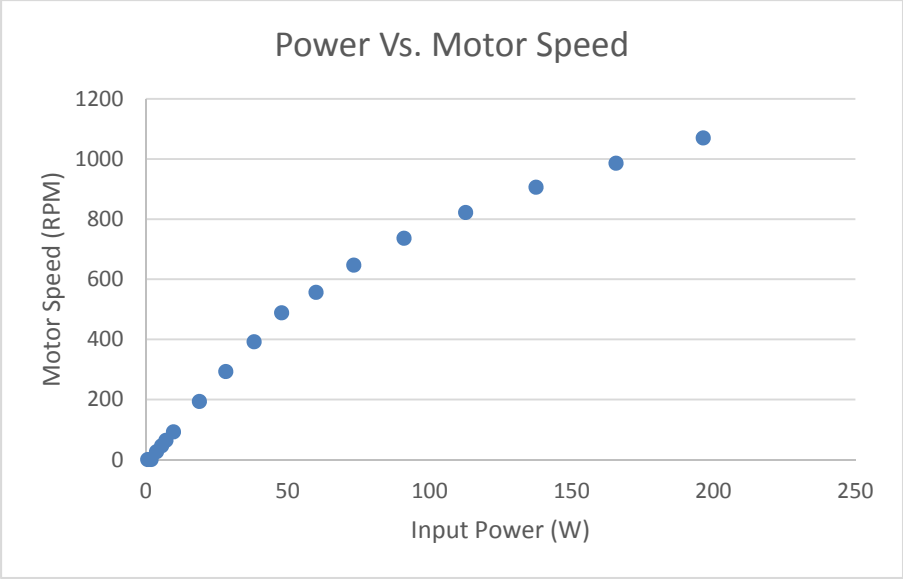

Figure 19: Input Power verses Speed of the Motor measured with a tachometer

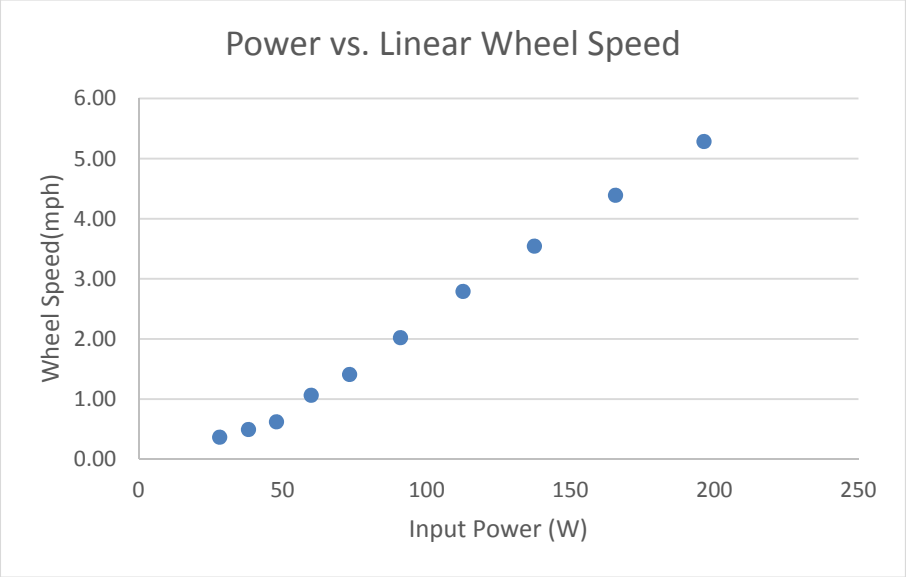

Figure 20: Input Power verses speed of the vehicle measured with a tachometer

The CVT changes the vehicle's gear ratio in order to adjust the speed and torque of the vehicle as motor speed changes. This accounts for the linearity of the power vs. linear wheel speed plot.

Section 5.4: Endurance Testing (No Load)

The endurance test was run at the same time as the heat displacement testing. This test simply measured the amount of time that the vehicle could run until the battery voltage level dropped below a "low" threshold. A battery can be drained to 40% of its total voltage, but there is a rapid decrease in voltage after the battery is discharged past a certain point. The measured discharge rate is shown in Figure 21.

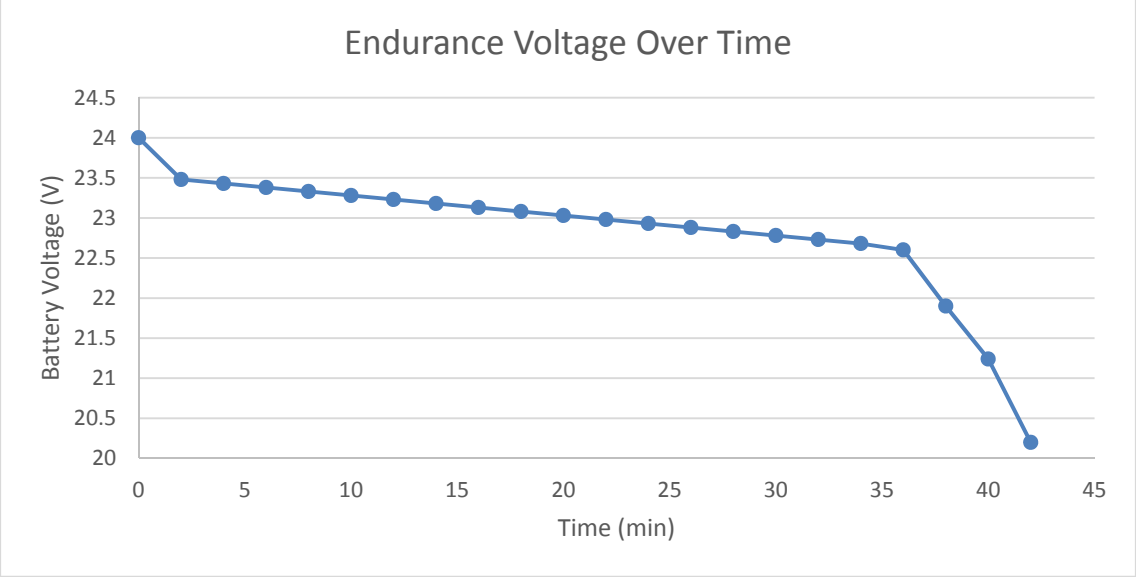

Figure 21: Voltage output from the batteries as time passed

The test was stopped after the battery output dropped below 20 volts to avoid damaging the batteries. This happened at the 43 minute mark. As the battery voltage dropped below 21 volts, the speed of the vehicle dropped rapidly. This speed change is shown in Figure 22.

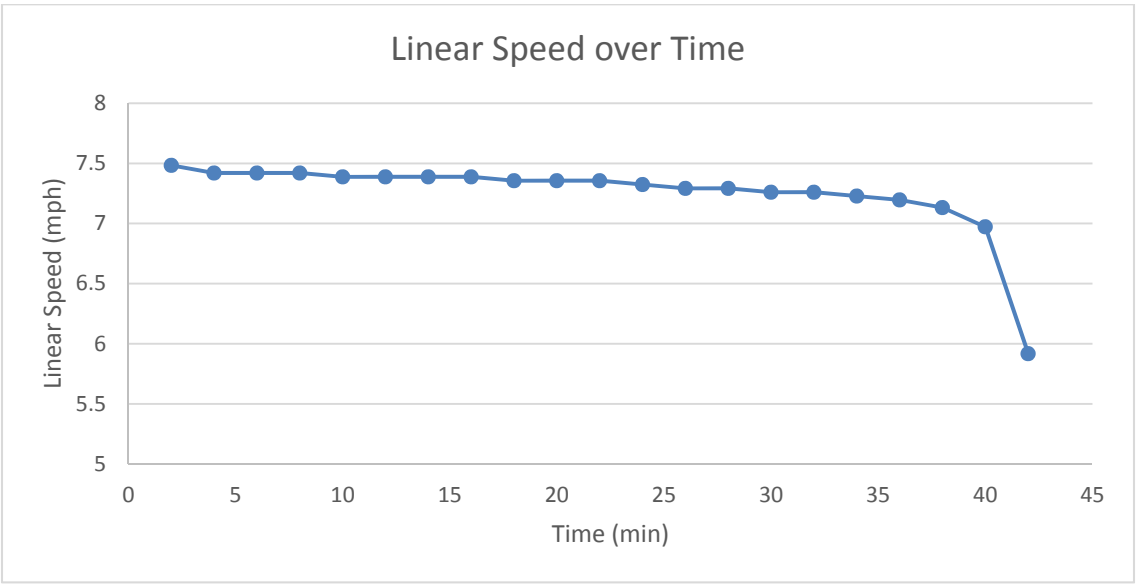

Figure 22: Linear speed of the vehicle over time

Section 5.5: Cooling System Testing

The problem statement of the project defined that the cooling system must keep all components under their respective thermal ratings and within optimal operating

temperatures. The batteries were identified as the only heat producing components within the EV requiring a cooling system. This was due to other components, like the DC-DC Converter and motor, supplied by the manufacturer with built-in heat dissipation devices. The purpose of the cooling system test was to verify the temperature of the batteries did not rise above their operating temperature for optimal efficiency during operation. Also, the efficiency of the cooling system was evaluated by comparing the heat dissipated by the fins and fans to the heat generated by the batteries. The data was then compared to the heat dissipated by the terminals without the cooling system.

The cooling system test was conducted in ET 105 of the IPFW Engineering and Technology Building using the following materials and equipment:

- (4) Type T Thermocouples
- Triplett 9055 Digital Multimeter/thermocouple reader
- (2) UB12500 Batteries
- (4) Aluminum fins structures
- (4) 120 mm Sleeve Bearing Silent Fans by Cooler Master
- IPFW Electric Vehicle

From the specification sheet for the UB12500 batteries, the maximum operating temperature for optimal efficiency was defined as 113° F and the internal resistance was 11 mΩ. The Triplett Digital Multimeter provided the temperature in ° F with a resolution of .1° F. The fans produced a volumetric flow rate of 44 cfm and pulled .15 Amps at 12 Volts from the batteries. This flow rate is only consistent through the cross sectional area of the fan opening and not the cooling system enclosure. The velocity of air passing over the fins were measured directly with an anemometer.

In order to collect the temperature readings of the fins during operation, Type T thermocouples were used to get accurate temperature reading of each terminal. Once the thermocouples were created, they were tested for functionality. One end was connected to the Triplett Digital Multimeter and the other submerged in ice water. If the thermocouple reader outputted a value other than 32° F, then the thermocouple was not considered operational and discarded.

Individual data was collected for each aluminum fin structure due to the fact that the contact resistance would vary amongst the four lead terminals. Thermocouples were inserted into the heat sinks and secured in place with thermal epoxy. The thermal compound of the adhesive promoted effective conductive heat transfer between the thermocouples and aluminum fins. Figure 23 shows the test setup for cooling system testing.

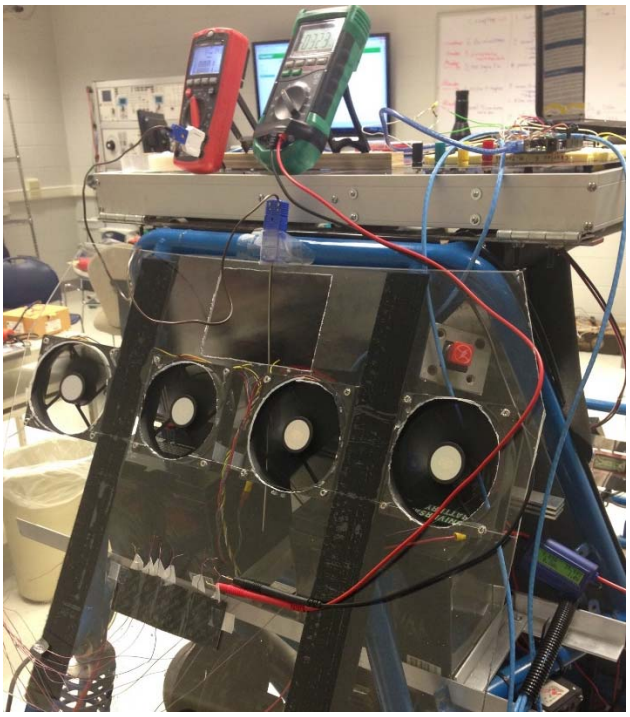

Figure 23: Setup of the cooling system testing conducted in Lab ET 105

The initial testing of the cooling system was conducted indoors under a no load condition. The electric vehicle was supported in a manner which kept the wheels elevated off of the ground. This condition allowed the motor to operate at a minimal torque since it was not required to overcome the force of the friction from the ground. The experiment was considered a “no load” condition; however, the load of the transmission and tires contributed to the heat generated by the batteries.

Throughout the experiment, the ambient temperature of the lab was collected using the built in temperature sensor of the thermocouple reader. The thermocouple used to collect the ambient temperature was placed inside the cooling system enclosure. The electric motor was set at its maximum speed of 1100 rpms and temperature measurements were recorded using the thermocouple reader at a time interval of 2 minutes for a duration of 40 minutes. The wheel speed (rpm), motor speed (rpm), and battery current (A) were also recorded at each interval.

Graphs of the terminal temperatures with respect to time are presented in Figure 24, Figure 25, Figure 26, and Figure 27.

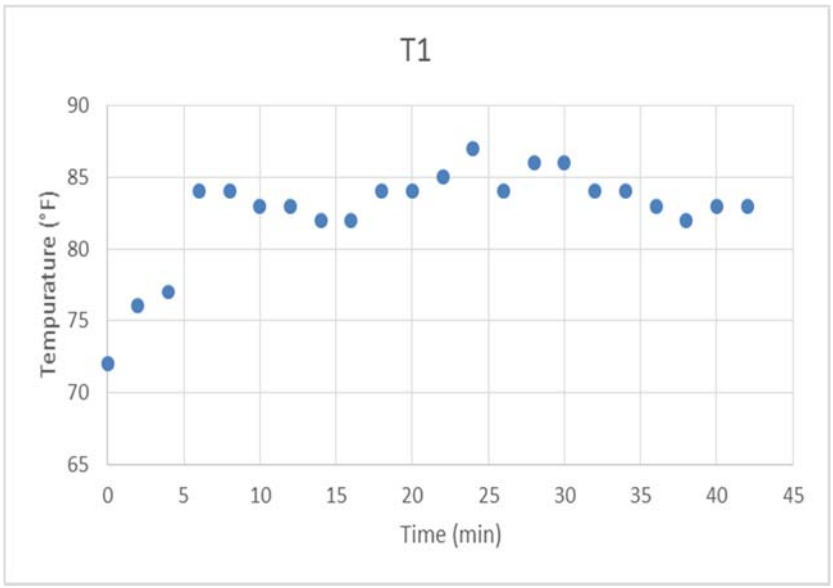

Figure 24: Battery 1, Negative Terminal

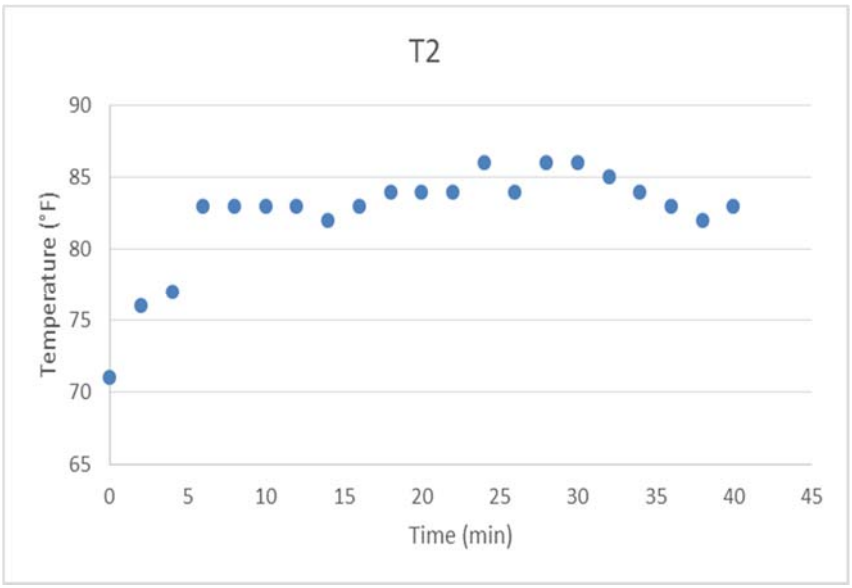

Figure 25: Battery 1, Positive Terminal

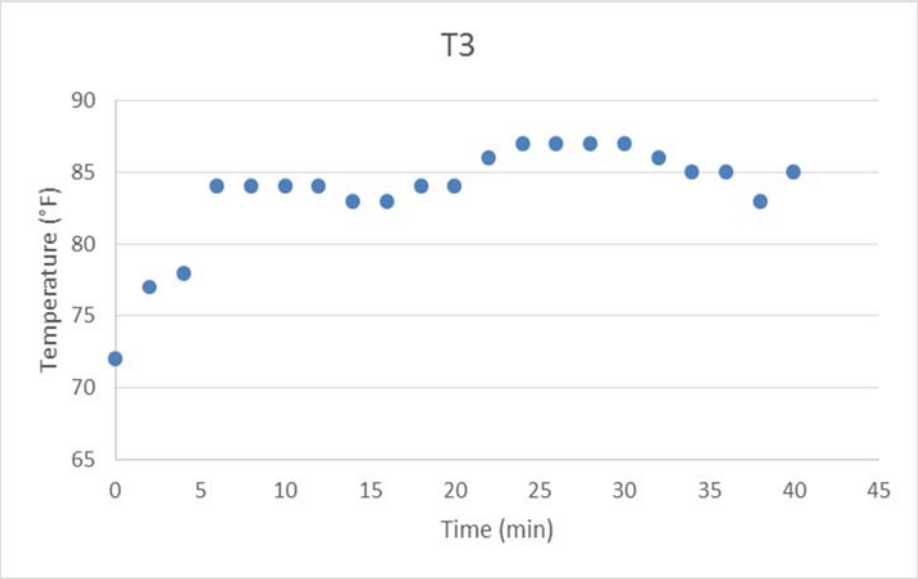

Figure 26: Battery 2, Negative Terminal

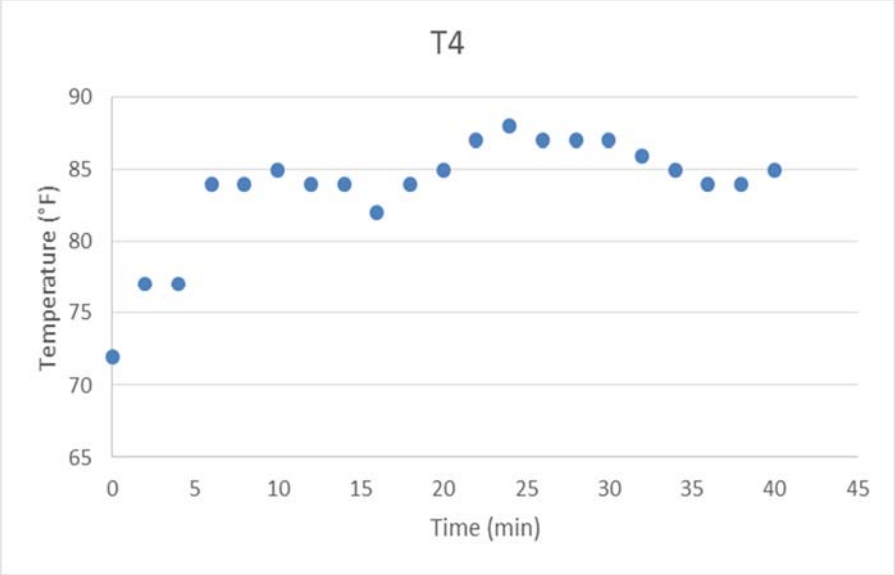

Figure 27: Battery 2, Positive Terminal

Within the first several minutes, the temperature increased at a high rate, but quickly stabilized for the remainder of the test. The highest thermocouple reading of 87 ° F was produced by the negative lead of the first battery at 24 minutes (Figure 23). This value was well below the maximum operating temperature for optimal efficiency of 113° F.

The variables involved in the analysis and calculations of the heat dissipated by the system are provided in Table 1Table 8**.**

Table 8: Nomenclature

Variable	**Descriptions**	**Units**

V	Velocity of Air	$\frac{m}{s}$
$\dot{v}$	Volumetric Flow Rate	$\frac{m^3}{s}$
A	Flow Area	m^2
A_f	Fin Surface Area	m^2
A_b	Prime Surface Area	m^2
Pr	Prandtl Number	-
w	Fin Width	m
L	Fin length	m
t	Thickness of the fin	m
Q	Heat transfer rate	W
$\bar{h}$	Convective Heat Transfer Coefficient	$\frac{W}{m^2k}$
K	Thermal Conductivity	$\frac{W}{mk}$
N	Number of Fins	-
T_∞	Ambient Temperature	°C
T_∞	Base of Fin Temperature	°C
η_f	Efficiency of the Fin	-
v	Kinematic Viscosity	m^2/s

In order to calculate the forced convection, the velocity of the air produced by the fans, V, was found by placing an anemometer within the flow area of the cooling system. The anemometer rotated at 60 RPM which correlates to a velocity of 0.214 m/s.

V = 0.214 m/s

Next, thermal properties for air at an average temperature, T_{avg}, were defined for the thermal conductivity, K, Prandl Number, Pr, and kinematic viscosity, v, in Table 9. Average temperature is defined as the average between the maximum base temperature of the battery terminals and the ambient temperature within the cooling area.

Table 9: Thermal Properties of Fin & Air

Air:	
T_{avg} (C)	27
K (W/mK)	.0261
Pr	.712
v (m^2/s)	1.576 E -05

The flow was identified as turbulent or laminar for the sides of the fin structures using the Reynold's Number. The Reynold's Number in Equation 24 is the ratio of inertial to viscous forces of the flow. It was calculated using the velocity of air produced by the fans, the length of the side of the fins parallel to the flow, and the kinematic viscosity, v, of the air at T∞.

$$Re_w = \frac{V * w}{v} \qquad \textbf{Eq. 24}$$

$$Re_w = \frac{(0.214\ {}^{m}/_{s})*(.023\ m)}{(1.576\ x10^{-5}\ {}^{m^2}/_{s})}$$

$$Re_w = 312.31$$

Since $Re_a < 5\ x10^5$ then the flow is laminar. Equation 25 is the average Nusselt Number correlation for forced convection with external parallel flow on a flat surface that is laminar.

$$\overline{Nu_w} = .664*P_r^{\frac{1}{3}}*Re_w^{\frac{1}{2}} \qquad \textbf{Eq. 25}$$

$$\overline{Nu_w} = .664*(.712)^{\frac{1}{3}}*(312.31)^{\frac{1}{2}}$$

$$\overline{Nu_w} = 10.478$$

In order to calculate the heat transfer coefficient, the definition of the average Nusselt Number was used in Equation 26. The equation holds true for laminar flow, with a Pr ≥ 0.6.

$$\overline{Nu_w} = \frac{\bar{h}*w}{k} \qquad \textbf{Eq. 26}$$

$$10.478 = \frac{\bar{h}*(.023\ m)}{(.0261\ \frac{W}{mK})}$$

$$\bar{h} = 11.89\ \frac{W}{m^2K}$$

The heat dissipated by the cooling system during the test was calculated using Equation 27 for heat dissipated by fins.

$$\mathrm{Q} = \mathrm{N}\mathrm{n_f}\mathrm{h}\mathrm{A_f}\theta_\mathrm{b} + \mathrm{h}\mathrm{A_b}\theta_\mathrm{b} \quad \textbf{Eq. 27}$$

The efficiency of the fin was calculated using Equation 28.

$$n_f = \frac{\tan h(m * Lc)}{m * Lc} \quad \textbf{Eq. 28}$$

The constant, m, was found using Equation 29.

$$m = \sqrt{\frac{2 * \mathrm{h}}{K * t}} \quad \textbf{Eq. 29}$$

$$m = \sqrt{\frac{2 * \left(11.89 \, \frac{W}{m^2 K}\right)}{\left(167 \, \left(\frac{\mathrm{W}}{\mathrm{mK}}\right)\right) . 003 \, m}}$$

$$m = 6.889$$

The constant, Lc, was found using Equation 30.

$$\mathrm{Lc} = \mathrm{L} + \frac{\mathrm{t}}{2} \quad \textbf{Eq. 30}$$

$$\mathrm{Lc} = .07 \ \mathrm{m} + \frac{.003 \ \mathrm{m}}{2}$$

$$\mathrm{Lc} = .072 \ \mathrm{m}$$

These constants were entered into Equation 31 to solve for the efficiency.

$$n_f = \frac{\tanh(6.889 * 072 \ \mathrm{m})}{(6.889) * (.072 \ \mathrm{m})} \quad \textbf{Eq. 31}$$

$$n_f = .93$$

Using Equation 32, the constant, θ_b, was solved for using the ambient temperature of the room and maximum base temperature found in the test.

$$\theta_b = T_b - T_\infty \quad \textbf{Eq. 32}$$

$$\theta_b = 30.5°\mathrm{C} - 23.6°\mathrm{C}$$

$$\theta_b = 6.9°\text{C}$$

Values were entered into Equation 27 for heat dissipated by heat sink below:

$$Q = (6)(.93)\left(11.89\ \frac{W}{m^2K}\right)(.003\ m)(6.9°\text{C}) + (11.89\ \frac{W}{m^2K})(.001\ m)(6.9°\text{C})$$

$$Q_{diss} = 1.455\ \text{W}$$

The cooling system consisted of two heat sinks; therefore, this value was multiplied by two to produce a total Q_{diss} of 2.911 Watts per battery.

The internal resistance and current generated by the two batteries were input into Equation 34 to provide the heat generated during the no load test.

$$Q_{gen} = I^2R \qquad \textbf{Eq. 34}$$

$$Q_{gen} = (13\ A)^2(.031\Omega)$$

$$Q_{gen} = 5.239\ W$$

The comparison of these two values are shown in Table 10.

Table 10: Cooling System Data for No Load

Q (W), Generated	Q (W), Experimental
5.239	2.911

The base temperature of the battery terminals without the cooling system was collected and compared to the no load test of the cooling system. Upon removing the fins from the terminals, a thermocouple was applied directly to the fin surface using thermal epoxy. Data was only collected from a single battery lead in this experiment because all the leads produce the same temperatures due to the absence of contact resistances. The experiment was conducted using the same method and procedures as the no load cooling system test. The electric motor was set at its maximum speed of 1100 RPM and temperature measurements were recorded using the thermocouple reader at a time interval of 2 minutes for a duration of 40 minutes. The ambient temperature of the lab, wheel speed (RPM), motor speed (RPM), and battery current (A) were recorded at each interval.

The cooling system was tested outdoors using the same equipment, methods, and procedures as the no load condition. The only variation to the loaded test were the intervals at which data was collected. Upon achieving a full charge in both batteries, the vehicle was relocated outdoors and tested on a flat, asphalt surface. The temperatures of the thermocouples were collected at three intervals listed below:

- Fully charged batteries (t=0 min)
- Half charged batteries
- Drained batteries (t~10 min)

The ambient temperature was also recorded at 46° F. The data from this experiment is provided in Table 11.

Table 11: Loaded Thermocouple Readings

	Temperature (°F)		
Battery 1, Negative Terminal	61	52	54
Battery 1, Positive Terminal	59	51	53
Battery 2, Negative Terminal	59	52	54
Battery 2, Positive Terminal	58	55	53

From the results of the no load testing of the cooling system, it was discovered that the heat generated contradicted the dissipated heat calculated experimentally. Figure 24, Figure 25, Figure 26, and Figure 27 show that the fins reached steady state after approximately 5 seconds. At steady state, heat generated is equal to the heat dissipated. The discrepancy between the generated and dissipated heat is most likely due to an increase in the internal resistance of the batteries to a value greater than the specified $.011\Omega$. Internal resistance increases as the age of a battery increases; and the UB12500 batteries used in this experiment were greater than three years old.

Since very little torque was applied to the system, very little current was pulled from the batteries and the maximum temperature achieved by the no load indoor test is not an accurate representation of the maximum temperature that can be seen in a more realistic environment. However, the indoor test does represent accurate performance of the cooling system when compared to the test where no cooling system was applied. The longer duration time of 40 minutes may also be attributed to this factor.

The thermocouple readings of the loaded experiment produced an even lower value for the heat removed than the no load condition. While there was a larger amount of current being pulled from the batteries to provide torque to the motor, the ambient temperature outside was considerably low, thus maintaining a low temperature in the fins.

The initial conditions during the loaded test, did not produce data comparable to the theoretical calculations. The experiment was conducted immediately upon introducing the vehicle to the outdoor temperature instead of waiting until they reached ambient temperature. As a result, the temperatures listed in Table 11 decrease as they cooled

off prior to increasing with operation. Few data points were collected during the experiment due to the inability to effectively monitor the temperature of the fins with a moving vehicle compared to the stationary vehicle of the no load condition. The loaded vehicle also had a very short operating time of less than 10 minutes due to the load on the system. The fins would have reached a higher temperature and achieved steady state had the run time been longer.

Both the no load and load cooling test produced valuable results as they demonstrated that the cooling system maintained battery temperatures below the maximum operating temperature of 113° F.

Section 5.6: Outdoor Testing (Load)

Outdoor speed and acceleration testing is done by placing the vehicle (with two batteries at full charge) outside on a flat surface and pressing the pedal fully down until the vehicle speed no longer increases. This yields both maximum acceleration and maximum speed. Figure 28 is a plot of the data from this test. Maximum speed is 2.37 mph, or 1.06 m/s. Maximum acceleration is calculated using a trendline with an R^2 value of 0.96 to be 0.0815 m/s^2.

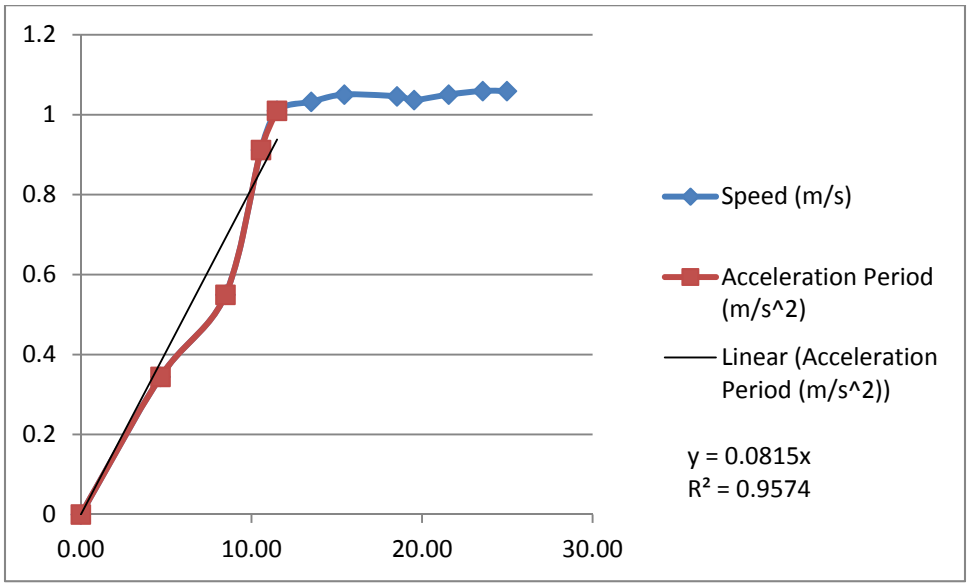

Figure 28: Speed (m/s) versus time (s)

After obtaining the maximum speed and maximum acceleration, the vehicle is run at maximum speed until it begins to slow. The entirety of the running time of the vehicle on a full battery charge using two batteries is measured to be seven minutes. (This short run time is diagnosed in the evaluation and recommendations.)

Section VI: Cost Analysis

After completing the Electrical Vehicle, the budget of $600 was exceeded by $1,440.25. A breakdown of the cost and items ordered are provided in Table 12.

Table 12: Cost Analysis

Part No.	Description	Manufacturer	Vendor	Unit Cost	Qty.	Total Cost
3G2425	Motor mount	3G Concepts, LLC.	3G Concepts, LLC.	$280.37	1	$280.37
1619	Heat shrink tube A	D.I.Y. It! Electronics	D.I.Y. It! Electronics	$12.99	1	$12.99
IR2110PBF-ND	IC driver high/low side 14dip	Digi-key	Digi-key	$4.14	5	$20.70
IR2110PBF-ND	IC driver high/low side 14dip	Digi-key	Digi-key	$4.14	4	$16.56
073854152400-140	Super glue, 2 pk.	Dollar General	Dollar General	$1.00	2	$2.00
-	8" color LCD display (w extra touch panel)	EastRising Technology Co., Ltd.	EastRising Technology Co., Ltd.	$101.31	1	$101.31
138081	6mm Zinc-Plated Metric Hex Nuts, 5 Ct.	HILLMAN GRP	Lowe's	$0.68	1	$0.68
138409	6-mm-1.0 x 20-mm Zinc Plated Metric Hex Bolts, 4 ct.	HILLMAN GRP	Lowe's	$0.92	1	$0.92
64171	Hardware 4-in Heavy T-Hinge Zinc	STANLEY	Lowe's	$3.67	1	$3.67
48536	1-5/16-in-2-1/4-in dia Stainless Steel Adjustable Clamps	Lowe's	Lowe's	$2.27	1	$2.27
136093	Ring wire connectors, 20 ct.	IDEAL	Lowe's	$4.48	1	$4.48
55817	1/4"-20 x 3/4" Zinc-SAE Hex Bolt	HILLMAN GRP	Lowe's	$0.05	4	$0.20
69725	4' x 1-1/4" HR Weldable Steel Metal Flat Bar	HILLMAN GRP	Lowe's	$7.19	1	$7.19
80887	3/4" 1-1/2" dia SS Adjustable Clamps, 2 pk.	Lowe's	Lowe's	$1.91	2	$3.82
163545	7" Nylon cable ties, 50 ct.	CATAMOUNT	Lowe's	$4.97	1	$4.97
135682	Butt splice wire connectors, 20 ct.	IDEAL	Lowe's	$2.58	1	$2.58
136010	Disconnects wire connector	IDEAL	Lowe's	$2.98	1	$2.98
157836	Load center wire marker booklet	GB	Lowe's	$9.47	1	$9.47
147965	100' 24/4 CAT 5E riser gray data cable	Lowe's	Lowe's	$18.47	1	$18.47
57848	#8-32 x 1-3/4" Round-head machine screws, 6 ct.	HILLMAN GRP	Lowe's	$0.98	1	$0.98
57819	#6-32 x 1/2" Round-head SAE machine screws, 14 ct.	BLUE HAWK	Lowe's	$0.98	2	$1.96

48536	1-15/16" 2-1/4" diam. SS, Adjustable Clamps, 2 ct.	HILLMAN GRP	Lowe's	$2.27	1	$2.27
63324	3/8" 16 x 1-1/2" SAE hex bolt	HILLMAN GRP	Lowe's	$0.18	2	$0.18
63317	5/16" 18 x 1" SAE hex bolt	HILLMAN GRP	Lowe's	$0.10	1	$0.10
228554	9' x 12' Plastic crop cloth	Lowe's	Lowe's	$1.98	1	$1.98
20934	Epoxy instant mix	LOCTITE	Lowe's	$3.77	1	$3.77
48144	1/2" Split flex tubing	IDEAL	Lowe's	$2.48	2	$4.96
409494	1/2" Pan-head SS SAE machine screws	HILLMAN GRP	Lowe's	$1.98	1	$1.98
57818	#6-32 x 3/8" Roung-head, Ct. 14	HILLMAN GRP	Lowe's	$0.98	2	$1.96
57863	#10-24 x 2" Roung-head, Ct. 5	Blue Hawk	Lowe's	$0.98	1	$0.98
57858	#10-24 x 1/2" Roung-head, Ct. 10	HILLMAN GRP	Lowe's	$0.98	1	$0.98
184582	Velcro industrial strength 4 x 2 tape box, white	VELCRO	Lowe's	$8.97	1	$8.97
40898	Velstrap 27 x 1 Straps, Ct. 2, black	VELCRO	Lowe's	$5.47	2	$10.94
57842	#8-32 x 3/8" Roung-head, Ct. 12	HILLMAN GRP	Lowe's	$0.98	1	$0.98
44159	3' x 1-1/4" HR weldable steel metal flat bar	HILLMAN GRP	Lowe's	$8.24	2	$16.48
48536	1-5/16"-2-1/4" dia SS adjustable clamps, 2 pk.	Lowe's	Lowe's	$2.27	2	$4.54
308977	zinc-plated door hinge	GATEHOUSE	Lowe's	$3.67	2	$7.34
63479	1/4" 20 x 5" (SAE) Hex Bolt	HILLMAN GRP	Lowe's	$0.24	9	$2.16
63408	1/4" SAE Split Lock Washer	HILLMAN GRP	Lowe's	$0.03	10	$0.30
63301	1/4" SAE Hex Nut	HILLMAN GRP	Lowe's	$0.03	10	$0.30
3440T15	6 x 19 Steel wire rope, 3/16" diam.	MCMASTER-CARR	MCMASTER-CARR	$0.84	20	$16.80
98830A200	Steel oversized keystock, 1/4" x 1/4" x 12"	MCMASTER-CARR	MCMASTER-CARR	$1.44	1	$1.44
30325T62	Cast malleable iron wire rope clip, 3/16" diam.	MCMASTER-CARR	MCMASTER-CARR	$0.60	4	$2.40
3256K14	Step-up shaft adapter for 7/8" x 1-1/8"	MCMASTER-CARR	MCMASTER-CARR	$63.24	1	$63.24
1497K145	Fully keyed 1045 steel drive shaft, 1" OD	MCMASTER-CARR	MCMASTER-CARR	$24.09	1	$24.09
61005K166	One piece clamp-on rigid shaft coupling	MCMASTER-CARR	MCMASTER-CARR	$66.08	1	$66.08
4334316	30" x 60" x 0.118", acrylic sheet	Menards	Menards	$44.98	1	$44.98
4334332	18" x 24" x 0.100", acrylic sheet	Menards	Menards	$9.78	1	$9.78

2018155	5/32" x 1-5/16" x .023 WG Compression spring	Menards	Menards	$0.59	1	$0.59
2026997	3/4" x 10-1/2" Compression spring	Menards	Menards	$3.49	1	$3.49
2018485	3/16" x 1-1/2" x .020 WG Compression spring	Menards	Menards	$0.59	1	$0.59
2026996	5/8" x 10-1/2" Compression	Menards	Menards	$3.19	1	$3.19
2323981	Grip Fast #8 Flat Washer, 75 pc.	Menards	Menards	$0.99	1	$0.99
2338563	Grip Fast 5/32" X 1" Slotted/Phillips Machine Screw , 11 pc	Menards	Menards	$0.82	1	$0.82
2026927	3mm-0.50 x 6mm Phillips Pan Machine Screws, 2 pcs.	Menards	Menards	$0.29	2	$0.58
2027054	1/2" x 1-1/4" Torsion, 1 pc	Menards	Menards	$1.39	1	$1.39
2015695	Nylon Spacer .140X1/4X 1/2	Menards	Menards	$0.69	5	$3.45
2015996	Nylon Spacer .171X3/8X 1/2	Menards	Menards	$0.69	2	$1.38
2015909	Nylon Spacer .171X3/8X 1/4	Menards	Menards	$0.69	2	$1.38
6790623	1-3/4" -2-3/4" Hose Clamp	Menards	Menards	$1.09	2	$2.18
2329734	Grip Fast 1/4"-20 Zinc Lock Nut W/Nylon Insert, 12 pc	Menards	Menards	$0.89	1	$0.89
2326022	Grip Fast 1/4" Zinc Split Lock Washer, 185 Pieces	Menards	Menards	$1.99	1	$1.99
2322281	Grip Fast 1/4"-20 x 1" Zinc-Plated Hex Bolts, 58 pc.	Menards	Menards	$1.89	1	$1.89
6790616	3/4"-1-3/4" Hose Clamp	Menards	Menards	$0.98	1	$0.98
2321017	Grip Fast 5/16"-18 Zinc Hex Nut, 11 oc.	Menards	Menards	$0.99	1	$0.99
AF6061/316112	Aluminum flat 6061T6, .188" x 1.5"	Metal Supermarkets	Metal Supermarkets	$0.11	57	$6.29
AA6061/1118	Aluminum angle 6061T6, 1" x 1" x .125"	Metal Supermarkets	Metal Supermarkets	$0.09	87	$7.79
AA6063/1212116	Aluminum angle 6061T5, .5" x .5" x .063"	Metal Supermarkets	Metal Supermarkets	$0.08	72	$6.00
SQ34	4" x 4" x 1' 6061-T6 Aluminum square	Metals Depot	Metals Depot	$106.83	1	$106.83
S113	13 Ga. (.105 thick) HR steel sheet	Metals Depot	Metals Depot	$58.50	1	$58.50
CCG304815S	30W 24/48Vin TDK-Lambda isolated DC/DC converter	Mouser Electronics	Mouser Electronics	$58.32	1	$58.32

	motor controller	RobotEQ.com	RobotEQ.com	$356.88	1	$356.88
-	8' Module	Schenzhen Square Electronics	Schenzhen Square Electronics	$51.98	1	$51.98
-	8 Touch panel w/ driver board	Schenzhen Square Electronics	Schenzhen Square Electronics	$14.92	1	$14.92
COM-10932	Rotary encoder - 200 P/R	Sparkfun Electronics	Sparkfun Electronics	$39.95	1	$39.95
ROB-09238	Stepper motor w/ cable	Sparkfun Electronics	Sparkfun Electronics	$14.95	1	$14.95
SEN-10988	Temperature sensor - TMP36	Sparkfun Electronics	Sparkfun Electronics	$9.00	6	$54.00
LCD-00256	Basic 20 x 4 character LCD, black on green, 5V	Sparkfun Electronics	Sparkfun Electronics	$21.94	1	$21.94
COM-08643	Magnet square - 0.25"	Sparkfun Electronics	Sparkfun Electronics	$1.50	1	$1.50
COM-10601	Reed switch - insulated	Sparkfun Electronics	Sparkfun Electronics	$1.95	1	$1.95
R4-S2S-124K-GP	Sleeve bearing 120mm silent fan for computer cases, 4 pk.	Cooler Master	NEWEGG	$12.49	1	$12.49
AS5-3.5G	5 High-density polysynthetic silver thermal compound	Arctic Silver	NEWEGG	$6.49	1	$6.49
615326	16 Tooth, 32 pitch, 4mm bore, pinion gear	Servocity	Servocity	$7.99	1	$7.99
32P-125-12	32 Pitch gear rack	Servocity	Servocity	$9.95	1	$9.95
-	Shipping and handling	Servocity	Servocity	$6.99	1	$6.99
100422	Disconnect wire connectors, 16 ct.	IDEAL	Lowe's	$2.98	1	$2.98
72685	6-AWG Stranded Black Copper THHN Wire (By-the-Foot)	Lowe's	Lowe's	$0.89	2	$1.78
72687	6-AWG Stranded Red Copper THHN Wire (By-the-Foot)	Lowe's	Lowe's	$0.89	8	$7.12
423948	20-Count Ring Wire Connectors	Utilitech	Lowe's	$2.97	1	$2.97
72529	10-AWG Stranded Black Copper THHN Wire (By-the-Foot)	Southwire	Lowe's	$0.49	2	$0.98
3641012	Thermal compound, 5g tube	Best Buy	Best Buy	$10.99	2	$21.98
163451	16G, black, 30 ft.	Primary wire	Autozone	$6.99	1	$6.99
412546	3A Blue LED, round rocker switch	Autozone	Autozone	$4.89	1	$4.89
32339	AGC low amp fuse, 10 Ct.	Bussman	Autozone	$3.99	1	$3.99
32422	HMK in-line fuse holder	Bussman	Autozone	$ 2.69	1	$ 2.69
2989273686	Side terminal	Walmart	Walmart	$1.94	1	$1.94
336624	12-Ct #10 SS Stand. (SAE) Hex Nuts	The Hillman Group	Lowe's	$1.98	1	$1.98

409452	8-Ct #10-24 x 3/4-in Pan-Head SS (SAE) Machine Screws	The Hillman Group	Lowe's	$1.98	1	$1.98
383357	50-ft 10-AWG Stranded White Copper THHN Wire	Lowe's	Lowe's	$13.97	1	$13.97
3641233	Yellow Female Disconnect (16 pk.)	Menards	Menards	$1.16	1	$1.16
3692949	50' #14 Red Stranded THHN Building Wire	Menards	Menards	$8.67	1	$8.67
AATA-5G	Arctic Alumina Thermal Adhesive 5g	Arctic Silver	Amazon.com	$7.49	1	$7.49
-	Battery mount material	Metal Supermarkets	Metal Supermarkets	$11.00	1	$11.00
-	Battery mount material	Metal Supermarkets	Metal Supermarkets	$11.00	1	$11.00
-	MOSFETS	Mouser Electronics	Mouser Electronics	$60.00	2	$120.00
				Subtotal		$1,906.78
				Tax		$133.47
				Total		**$2,040.25**

Evaluation and Recommendations

The achieved results are compared against the requirements, specifications, limitations, and constraints. Recommendations for future improvements are given.

Evaluation

The specified batteries and DC motor work together to power the vehicle, as required. The solar panel can fully recharge two drained batteries in 20 hours. This is two hours longer than the specified time, but the time in the problem statement was based on maximum sun, and perfect conditions did not persist throughout the entirety of the test.

The electric vehicle can accelerate to a top speed of 2.37 mph in 11.5 seconds and can maintain this speed for seven minutes. Neither the specified speed (7 mph) nor the specified run time (60 minutes) was achieved.

There are at least four reasons for the low speed and run time: (1) The vehicle had just two batteries, instead of the five which the system can support, (2) the batteries in use had a lifespan of one year, but are three years old, (3) the front wheels are each splayed slightly outwards so that the front tires are fighting each other, causing unnecessary loss, and (4) the gearbox is set to a low gear, resulting in a high gear ratio.

The vehicle has an adjustable speed range. The achievement of various speeds is accomplished by the compression of a pedal in the lower front right of the vehicle; the same method used by almost every other four-wheeled vehicle.

As torque could not be measured due to the absence of the required tool(s), it is not possible to measure efficiency directly.

The cost of the vehicle significantly exceeded the $1,000 limit, coming to $2,040.25.

The interior dimensions of the vehicle allow a driver to operate the vehicle with comfort. The vehicle's weight, while over the specified value of 400 lb., is not unexpected for the frame and materials used. It does not prevent the vehicle from moving or accelerating.

The project was completed by December 2015 according to plan.

Recommendations

Due to the age of the two installed batteries, they should be replaced. In addition, three additional batteries should be purchased and installed to achieve the full capability of the system. Using five batteries instead of two will dramatically boost power, torque, acceleration, and speed.

For maximum battery life, an intelligent charging circuit should be designed and installed that charges each battery individually and stops when the battery is charged.

The alignment of the two front wheels should be adjusted in order to minimize friction and improve the performance of the vehicle.

The existing gearbox can only be put into low and reverse. A new gearbox should be purchased, or the current one repaired to allow for a high gear. A high gear will allow the vehicle to attain speeds even higher than those achieved by the addition of more batteries and the alignment of the front wheels.

There is vibration in the CVT and motor shaft. This vibration should be studied to determine which component or combination of components in the shaft coupling is creating it, and if it will create problems for the motor at its current amplitude. A flexible shaft coupling may help reduce this vibration if the vibration is coming from shaft misalignment.

References

Fundamentals of Heat and Mass Transfer, 7th edition, T. Bergman, A. Lavine, F. Incropera, D. DeWitt, May 2011.

Appendix A: Control System

Electric Vehicle Control System

$v = velocity\ of\ vehicle$

$\dot{v} = acceleration$ of vehicle

$\gamma = road\ friction\ proportional\ to\ velocity\ (parameter)$

$f =\ force\ moving\ vehicle\ forward$

$m = mass\ of\ vehicle$
$u = voltage\ provided\ to\ servo$

$c = electromechanical\ parameter$

Force moving vehicle due to our system's electromagnetic constant and supplied voltage:

$$f = cu$$

Newton's Law:

$$m\dot{v} = f - \gamma v$$

Laplace Transform:

$$msV(s) = cU(s) - \gamma V(s)$$

$$\frac{V(s)}{U(s)} = \frac{c}{ms + \gamma} = \frac{{}^{c}/_{m}}{s + {}^{\gamma}/_{m}} = \frac{{}^{c}/_{\gamma}}{{}^{m}/_{\gamma}\, s + 1} = \frac{{}^{c}/_{\gamma}}{{}^{m}/_{\gamma}\, s + 1} = \frac{K}{\tau s + 1}$$

$$\tau = time\ constant = {}^{m}/_{\gamma}$$

$$K = parameter = {}^{c}/_{\gamma}$$

Solving on Paper:

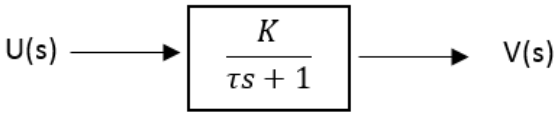

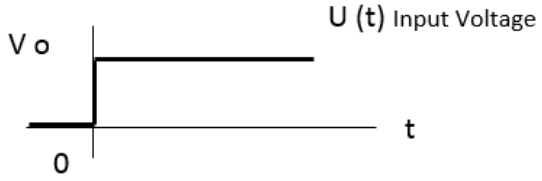

$Vo = applied\ voltage$

$$U(s) = \frac{Vo}{s}$$

$$V(s) = \frac{K}{\tau s+1} * \frac{Vo}{s} = \frac{KVo}{s(\tau s+1)} = KVo\left(\frac{1}{s} - \frac{\tau}{\tau s+1}\right)$$

$$V(t) = KVo\left(1 - e^{-t/\tau}\right), \qquad t \geq 0$$

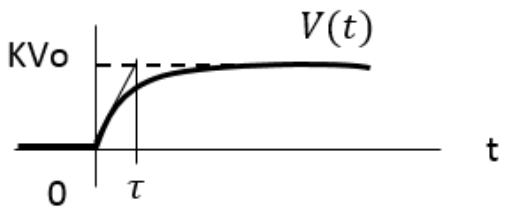

$$\frac{dV}{dt} = -KVo\left(-\frac{1}{\tau}e^{-\frac{t}{\tau}}\right) = \frac{KVo}{\tau}\left(e^{-t/\tau}\right)$$

$$\left.\frac{dV}{dt}\right|_{t=0} = \frac{KVo}{\tau} = \frac{rise}{run} = \frac{KVo}{t_1} \rightarrow t_1 = \tau$$

Practical Test:

1. Apply known voltage, Vo, and make measurement of the car speed
2. Plot and pass a curve through data points
3. Measure steady – state value, KVo.
4. Divide by Vo to get K.
5. Measure the slope of the curve. Divide KVo by slope and get τ.
6. Can also solve for c and γ.

$$\gamma = {}^{m}/_{\tau}$$

$$c = K\gamma$$

Appendix B: Power Operation Instructions

Instructions to turning on and off the vehicle

Before starting the vehicle, make sure all of the battery connections are tight and secure. If any of the connection is not secure, tighten it. An unsecure connection could cause a catastrophic failure in the system. Also make sure that you are not either pulling or pushing the pedal before starting the system, otherwise the system might underperform or run while the pedal is in the neutral position.

Turning the Vehicle On

1. Turn on the black switch, located in the back of the vehicle.
2. Turn on the switch in front of the vehicle, the switch must go all the way down. This switch has three states, but only two are meant to be used in this design, therefore always make sure that the switch is never on the middle state.
3. The LCD should turn and can be used as a reference that the system is on.
4. The gear the vehicle will run must be set before pressing the pedal. Forward right is the low-forward gear and forward right is the reverse gear.
5. Press the pedal and the vehicle will move.

Turing the Vehicle Off

1. Turn off the switch in the front of the vehicle.
2. Turn off the black switch, located in the back of the vehicle.

Appendix C: Motor Controller Settings

- Start-up
  - Scripting
    - Script Auto-Start: Enable
  - Analog Start-up
    - Center Command to Start: Enabled
  - Telemetry
    - Telemetry String:
- Commands
  - Command Priorities
    - Priority 1: Pulse
    - Priority 2: RS232
    - Priority 3: None
    - Default Command Value: 0
  - Command Adjustments
    - Linearity 1: Linear
    - Linearity 2: Linear
  - Command Safety
    - RS232 Safety
      - Watchdog (ms): 1000
    - Pulse Safety
      - Keep within Min/Max: Disabled
    - Analog Safety
      - Keep within Guard Bands: Enabled
- CAN
  - CAN Mode: Off
  - Bit Rate: 250
  - Node ID: 1
  - Listen Node ID: 4
  - Heartbeat (ms): 0
  - MiniCAN Send Rate (ms): 100
  - CANOpen Autostart: Disabled
- Encoder
  - Use: Disabled
  - Pulses/Rev: 100
  - Min Limit: -20000
  - Max Limit: 20000
  - Home Count: 0
  - Action at Min: No Action
  - Action at Max: No Action
- Digital Inputs
  - DIn1:
    - Active Level: High
    - Action: No Action
  - DIn2:
    - Active Level: High
    - Action: No Action
  - DIn3:
    - Active Level: High
    - Action: No Action
  - DIn4:
    - Active Level: High
    - Action: No Action
  - DIn5:
    - Active Level: High
    - Action: No Action
  - DIn6:
    - Active Level: High
    - Action: No Action

- Analog Inputs
  - AIn1:
    - Conversion Type: Disabled
    - Input Use: No Action
    - Range: Calibrate
      - Input Min (mV): 0
      - Input Center (mV): 0
      - Input Max (mV): 4750
    - Conversion Polarity: Direct
    - Input Deadband (%): 1
    - Action on Min: No Action
    - Action on Max: No Action
  - AIn2:
    - Conversion Type: Disabled
    - Input Use: No Action
    - Range: Calibrate
      - Input Min (mV): 250
      - Input Center (mV): 2500
      - Input Max (mV): 4750
    - Conversion Polarity: Direct
    - Input Deadband (%): 5
    - Action on Min: No Action
    - Action on Max: No Action
  - AIn3:
    - Conversion Type: Disabled
    - Input Use: No Action
    - Range: Calibrate
      - Input Min (mV): 250
      - Input Center (mV): 2500
      - Input Max (mV): 4750
    - Conversion Polarity: Direct
    - Input Deadband (%): 5
    - Action on Min: No Action
    - Action on Max: No Action
  - AIn4:
    - Conversion Type: Disabled
    - Input Use: No Action
    - Range: Calibrate
      - Input Min (mV): 250
      - Input Center (mV): 2500
      - Input Max (mV): 4750
    - Conversion Polarity: Direct
    - Input Deadband (%): 5
    - Action on Min: No Action
    - Action on Max: No Action
  - AIn5:
    - Conversion Type: Disabled
    - Input Use: No Action
    - Range: Calibrate
      - Input Min (mV): 250
      - Input Center (mV): 2500
      - Input Max (mV): 4750
    - Conversion Polarity: Direct
    - Input Deadband (%): 5
    - Action on Min: No Action
    - Action on Max: No Action
  - AIn6:
    - Conversion Type: Disabled
    - Input Use: No Action
    - Range: Calibrate
      - Input Min (mV): 250
      - Input Center (mV): 2500
      - Input Max (mV): 4750
    - Conversion Polarity: Direct
    - Input Deadband (%): 5
    - Action on Min: No Action
    - Action on Max: No Action
- Pulse Inputs
  - PIn1:
    - Capture Type: Duty Cycle
    - Input Use: Motor Command
    - Range: Calibrate
      - Input Min: 0
      - Input Center: 0
      - Input Max: 4500
    - Capture Polarity: Direct
    - Input Deadband (%): 5
    - Action on Min: No Action
    - Action on Max: No Action
  - PIn2:
    - Capture Type: Disabled
    - Input Use: No Action
    - Range: Calibrate
      - Input Min: 1000
      - Input Center: 1500
      - Input Max: 2000
    - Capture Polarity: Direct
    - Input Deadband (%): 5
    - Action on Min: No Action
    - Action on Max: No Action
  - PIn3:
    - Capture Type: Disabled
    - Input Use: No Action
    - Range: Calibrate
      - Input Min: 1000
      - Input Center: 1500
      - Input Max: 2000
    - Capture Polarity: Direct
    - Input Deadband (%): 5
    - Action on Min: No Action
    - Action on Max: No Action

- Pin4:
  - Capture Type: Disabled
  - Input Use: No Action
  - Range: Calibrate
    - Input Min: 1000
    - Input Center: 1500
    - Input Max: 2000
  - Capture Polarity: Direct
  - Input Deadband (%): 5
  - Action on Min: No Action
  - Action on Max: No Action
- Digital Outputs
  - DOut1:
    - Active Level: High
    - Activate when: Motor is On
  - DOut2:
    - Active Level: High
    - Activate when: No MOSFET Fail
- General
  - PWM Frequency (kHz): 16.0
  - Voltage Limits
    - Over Voltage Limit (V): 40.0
    - Under Voltage Limit (V): 5.0
  - Brake Delay (ms): 250
  - Short Circuit Protection: Medium
- Motor Configuration
  - Number of Pole Pairs: 12
  - Closed Loop Feedback Sensor: Hall Sensor
  - Stall Detection: 500ms @ 25% Power
  - Switching Mode: Trapezoidal
  - Hall Counter
    - Min Limit: -20000
    - Max Limit: 20000
    - Home Count: 0
    - Action at Min: No Action
    - Action at Max: No Action
- Sinusoidal Settings
  - Sinusoidal Angle Sensor: Encoder
  - Reference Seek Power (A): 20.0
  - Angle Timing Advance: 0
  - Angle Zero Adjust: 0
- Motor Output
  - Amps Limits
    - Amps Limit (A): 75.0
    - Amps Trigger (A): 75.0
    - Amps Trigger Action: No Action
    - Amps Trigger Delay (ms): 500
  - Power Adjust
    - Max Power Fwd (%): 100
    - Max Power Rev (%): 100
  - Speed & Acceleration
    - Max Speed (RPM): 5000
    - Acceleration (RPM/s): 500.0
    - Decceleration (RPM/s): 500.0
  - Operating Mode: Open Loop
  - Closed Loop Parameters
    - Position Mode Velocity (RPM): 1000
    - * Position Turns Min to Max: 555.54
    - Proportional Gain: .0
    - Integral Gain: 1.0
    - Differential Gain: .0
    - Integrator Limit (%): 100
    - Loop Error Detection: 500ms @ 25% Error

Appendix D: Arduino Code

```
// include the library code:
#include <LiquidCrystal.h>
#include "digitalWriteFast.h" // google this and install it

const byte pin_A =  2;       // white wire from wncoder
const byte pin_B =  3;       // black wire from encoder
const int voltageOut = 9;    //Output voltage towards converter
const int atempSensor = A14; //Ambient temperature sensor
const int reed       =  A0;  // Reed switch for the speed sensor

int curReedVal     = 0;
int tempcounter =   0;
int A_set =         0;
int B_set =         0;
long pulses =       0;
int encoderVal   =  0;
int ambtemp =       0;
int battemp =       0;
float mph =     0;
int current =       0;


//tire circumference 1.72 meters
// variables for speed sensor
//storage variables
int reedVal;
long timer;// time between one full rotation (in ms)
float circumference = 1.72;
//increasing the maxReed counter will decrease the max speed it will use
//decreasing the maxReed counter will increase the max speed it will use
int maxReedCounter = 80;//min time (in ms) of one rotation (for debouncing)
int reedCounter;



// initialize the library with the numbers of the interface pins
LiquidCrystal lcd(43, 45, 47, 49, 51, 53);



void setup() {

  // set up the LCD's number of columns and rows:
  lcd.begin(20, 4);
  lcd.clear();
  // Print a message to the LCD.
  lcd.print("Speed:");
  lcd.setCursor(0, 1);
  lcd.print("Ambient Temp:");
  lcd.setCursor(0, 2);
  /*
  lcd.print("Batt Life:");
  lcd.setCursor(0, 3);
  lcd.print("S:");
  lcd.setCursor(10, 1);
  lcd.print("BL:");
  lcd.setCursor(10, 2);
  lcd.print("C:");
```

```
  */

  pinMode(pin_A, INPUT);
  digitalWrite(pin_A, HIGH); // enables pull-up resistor
  pinMode(pin_B, INPUT);
  digitalWrite(pin_B, HIGH); // enables pull-up resistor

  A_set = digitalRead(pin_A);
  B_set = digitalRead(pin_B);

  attachInterrupt(0, encoderPinChange_A, CHANGE); // pin 2
  attachInterrupt(1, encoderPinChange_B, CHANGE); // pin 3

  reedCounter = maxReedCounter;
  pinMode(reed, INPUT);


  // TIMER SETUP- the timer interrupt allows precise timed measurements of the reed
switch
  cli();//stop interrupts

  //set timer1 interrupt at 1kHz
  TCCR1A = 0;// set entire TCCR1A register to 0
  TCCR1B = 0;// same for TCCR1B
  TCNT1  = 0;
  // set timer count for 1khz increments
  OCR1A = 1999;// = (1/1000) / ((1/(16*10^6))*8) - 1
  // turn on CTC mode

  TCCR1B |= (1 << WGM12);
  // Set CS11 bit for 8 prescaler
  TCCR1B |= (1 << CS11);
  // enable timer compare interrupt
  TIMSK1 |= (1 << OCIE1A);

  sei();//allow interrupts
  //END TIMER SETUP

  Serial.begin(9600);
}

void loop() {
  // set the cursor to column 0, line 1
  Serial.println(encoderVal);
  // Encoder value is changed to a pulse output
  encoderVal= (pulses *255)/-675;
  //Necessary measures are taken to make sure that the output
  //doesn't go higher or lower than what the output is rated at
  if (encoderVal < 5)
  {
    encoderVal=1;
  }
  if (encoderVal > 250)
  {
    encoderVal = 255;
  }
  analogWrite(voltageOut,encoderVal);
  lcd.setCursor(6, 0);
```

```
  lcd.print(mph);
  lcd.print("mph  ");
  ambtemp= ((analogRead(atempSensor)-154)*.49+25)*1.8+32;
  lcd.setCursor(13, 1);
  lcd.print(ambtemp);
  lcd.print("F  ");
    /*
    lcd.setCursor(3, 2);
    lcd.print(battemp);
    lcd.print("F  ");
    */
  /*
  lcd.setCursor(2, 3);
  lcd.print(mph);
  lcd.print("mph  ");
  lcd.setCursor(12, 2);
  lcd.print(current);
  lcd.print("A  ");
  */
  delay(1000);
}

void encoderPinChange_A()
{
  //If A is higher than B then increase the pulse count.
  A_set = digitalReadFast2(pin_A) == HIGH;
  pulses += (A_set != B_set) ? +1 : -1;
}


void encoderPinChange_B()
{
  //if B is higher than A then decreases the pulse count
  B_set = digitalReadFast2(pin_B) == HIGH;
  pulses += (A_set == B_set) ? +1 : -1;
}


ISR(TIMER1_COMPA_vect) {//Interrupt at freq of 1kHz to measure reed switch
  reedVal = digitalRead(reed);//get val of A0
  if (reedVal && (curReedVal==0)){//if reed switch is closed make sure it doesnt
    curReedVal = 1;
    if (reedCounter == 0){//min time between pulses has passed
      mph = (2237*float(circumference))/float(timer);//calculate miles per hour
      timer = 0;//reset timer
      reedCounter = maxReedCounter;//reset reedCounter
    }
    else{
      if (reedCounter > 0){//don't let reedCounter go negative
        reedCounter -= 1;//decrement reedCounter
      }
    }
  }
  else{//if reed switch is open
    if (reedVal == 0)
    {
      curReedVal=0;
    }
```

```
    if (reedCounter > 0){//don't let reedCounter go negative
      reedCounter -= 1;//decrement reedCounter
    }
  }
  if (timer > 5000){
    mph = 0;//if no new pulses from reed switch- tire is still, set mph to 0
  }
  else{
    timer += 1;//increment timer
  }
}
```